

Vortex dynamics of the two-dimensional turbulent shear layer

By HASSAN AREF AND ERIC D. SIGGIA

Laboratory of Atomic and Solid State Physics, Cornell University, Ithaca, NY 14853

(Received 18 June 1979 and in revised form 19 December 1979)

The role of large vortex structures in the evolution of a two-dimensional shear layer is studied numerically. The motion of up to 4096 vortices is followed on a 256×256 grid using the cloud-in-cell algorithm. The scaling predictions of self-preservation theory are confirmed for low-order velocity correlations, although the existence of vortex structures produces large fluctuations even in a simulation of this size. The simple picture of the shear layer as a line of vortex blobs, that merge pairwise thus thickening the layer, is not seen. On the contrary, the layer seems to thicken by the scattering of vortex structures of roughly fixed size about the midline. The size of the vortex structures does not scale with the layer thickness. A study of the entrainment of a passive marker shows that flow visualization experiments may have overestimated the size of the vortex structures. It appears that the finite area vortices have time to equilibrate between mergings, and the consequences of applying equilibrium statistical mechanics to their internal structure are explored. A simple model is presented which demonstrates how the size and separation of vortex structures may lock into a fixed ratio. This is precisely the type of mechanism that is needed to produce simple scaling in a flow that has initially several distinct length scales. A number of consistency checks on the numerical results are performed. In particular, the evolution of the same vortex configuration on two grids of different size is compared. This test showed that, although errors on subgrid scales do propagate to small wavenumbers, the dominant wavenumber of vorticity cascades back ahead of the peak in the error spectrum.

1. Introduction

Recent experiments on the plane turbulent mixing layer (Winant & Browand 1974; Brown & Roshko 1974) have substantially changed our picture of this simple free turbulent flow. The experiments show, contrary to most expectations, that the mixing layer is dominated by large, spanwise coherent vortex structures. They suggest that the downstream thickening of the turbulent mixing layer arises through sequential amalgamation of these vortices to form ever larger vortices. Winant & Browand (1974) referred to this process as vortex pairing, and Brown & Roshko (1974) actually produced a plot of vortex positions versus time, which shows the whole genealogy of the vortex structures, with vortices of one generation merging to form the larger vortices of the next generation. The reader is referred to Roshko (1976) for a review. A considerable amount of information on structures in turbulent flows is

contained in the Proceedings of the 1977 Berlin Symposium on Structure and Mechanisms of Turbulence (Fiedler 1978).

While all experiments that we are aware of support the existence of coherent structures in two-dimensional mixing layers, i.e. those in which the instantaneous large-scale velocity field is identically zero in the spanwise direction, turbulence in the absence of large-scale rotation or stratification generally appears to become three dimensional. When the two initial streams are not kept two-dimensional prior to merging the existence of structures downstream is more controversial. We refer the reader to the remarks made by Batt (1977) and the experiments of Chandrsuda *et al.* (1978). The recent investigation of Wygnanski *et al.* (1979) discusses the emergence and persistence of the two-dimensional structure in the mixing layer. These authors observe coherent structures as previously described under a variety of initial conditions, including fully turbulent boundary layers on the splitter plate and enhanced free-stream turbulence (see also Browand and Troutt 1980).

We shall consistently refer to the common laboratory case of the flow downstream from a splitter plate as the mixing layer. This flow is statistically stationary but it evolves downstream. A flow that starts as a tangential discontinuity of velocity across an infinite plane we shall designate a (unsteady) shear layer. This flow has statistical homogeneity along the layer. Traditional theories of these free turbulent flows based on Reynolds equations start from the notion of self-preservation (Monin & Yaglom 1971; Tennekes & Lumley 1972). To be specific, consider the unsteady shear layer with a velocity jump ΔU across the layer and a thickness $\theta(t)$ (for an exact definition see (3.3)) at very large Reynolds number. The velocity far above the layer is $-\frac{1}{2}\Delta U$, and far below is $\frac{1}{2}\Delta U$. Self-preservation theory asserts that if all velocities are scaled by ΔU , and all lengths perpendicular to the shear layer are scaled by $\theta(t)$, then the scaled flow is statistically stationary. For example, if y is the co-ordinate transverse to the shear layer and u is the velocity along the shear layer, the ensemble average, $\langle u \rangle$, of u depends only on y and time t , by statistical homogeneity along the layer, and is assumed to satisfy the scaling law

$$\langle u \rangle = \Delta U f(y/\theta(t)), \quad (1.1)$$

where f is some universal function in principle calculable from the equations of motion. In this same theory θ grows proportionally to $\Delta U t$. Our applications of self-preservation theory will be limited to the largest scales of the flow and to high values of Reynolds number.

Although they are often discussed together in the literature, the unsteady shear layer and the mixing layer are not rigorously equivalent in the sense that it is not possible to go from one to the other by a Galilean transformation. The difference is apparent when one applies self-preservation theory to the mixing layer. Let U_1 and U_2 be the free stream velocities on the two sides of a splitter plate, so that $\Delta U = U_1 - U_2$. The dimensionless ratio $\Lambda = (U_1 - U_2)/(U_1 + U_2)$ should in principle be included when writing down scaling laws. Self-preservation applied to the mixing layer will always give θ proportional to x , where θ is the layer thickness at station x downstream of the splitter plate, but the constant of proportionality depends on Λ (cf. Brown & Roshko 1974; Browand & Latigo 1979). For the shear layer, the constant of proportionality between $\theta(t)$ and $\Delta U t$, called r in (3.7) below, cannot depend on Λ since the statistics

of this flow are invariant under a Galilean transformation along the layer while Λ is not. Similarly, in the generalized version of (1.1),

$$\langle u \rangle - \frac{1}{2}(U_1 + U_2) = \Delta U f(y/\theta), \quad (1.2)$$

the ‘universal’ function f may depend on Λ for the mixing layer but not for the shear layer. Experimentally most if not all of the Λ dependence of f comes from the coefficient in the formula for the growth of θ with x (Browand & Latigo 1979). Thus, while there is just one self-preserving shear layer, the mixing layer really consists of a one-parameter family of flows. In this paper we study the two-dimensional shear layer. On physical grounds, we expect the shear layer and a given mixing layer to be similar since spreading angles are empirically small (cf. the discussion following (3.7) and the small value of r). Thus, at a point far downstream of the splitter plate the boundaries of the turbulent region in a mixing layer appear nearly parallel.

The discovery of vortex structures in the turbulent mixing layer raises serious doubts about the validity of self-preservation arguments. The idea that a mixing layer can be characterized statistically by just one length scale, although obviously approximate, is certainly much more plausible if the vorticity is spread out randomly within some wedge emanating from the trailing edge of the splitter plate. In a flow dominated by vortex roll structures the implication is that self-preservation is inadequate even as the lowest-order approximation. The flow visualization pictures of Brown & Roshko (1974), and later many others, present at least two dynamically significant length scales: the size and separation of the vortex structures. We emphasize, that the existence of structures *per se* is not sufficient to ruin simple scaling. For there may exist mechanisms that produce a locking of all relevant length scales into fixed ratios, leaving effectively only one length scale. Simple scaling then follows. Judging from the empirical success of the self-preservation results, mechanisms of this kind may be expected. Stated differently, if the large scales prove to be exactly self-similar, then they must be independent of Reynolds number, since in the shear layer Reynolds number grows linearly with $\theta(t)$. The other possibility is that there actually are several distinct length scales, but the violations of simple scaling, that they engender, are small and remain buried in experimental uncertainty. However, dynamical issues are involved here and some contact with the basic equations must be made. We shall return to this line of argument in §4. It is important to note that these questions of principle are present in two dimensions as well as in three.

An analogy with the dynamics of an isotropic, inertial subrange in three-dimensional turbulence should be noted. Again there is a simple scaling theory (Kolmogorov 1941) that assumes a single dynamically determined length, $(\nu^3/\epsilon)^{1/4}$, and a single wavenumber dependent characteristic velocity, $(\epsilon/k)^{1/3}$, where ϵ is the rate of dissipation and ν is the viscosity. (The conventional ‘ $-\frac{5}{3}$ spectral law’ follows by squaring this velocity, and differentiating once with respect to k to yield an energy spectrum.) This theory describes the energy spectrum very well, but fails to account correctly for higher-order correlation functions. At the phenomenological level (Kolmogorov 1962; Frisch, Sulem & Nelkin 1978) intermittency effects in three dimensions are modelled by superimposing a secular trend on Kolmogorov’s cascade process. In other words, the fluid ‘counts’ the number of cascade steps, $\sim \log_2(kL)$, between the current scale size k^{-1} and the largest scales L . In the shear-layer problem the hierarchy of vortex

mergings, i.e. the fusion of distinct islands of vorticity, defines an analogy of the cascade. Energy is of course now being shifted from smaller to larger scale sizes. Simple scaling, which like the Kolmogorov–Oboukhov theory ignores fluctuations associated with the spotty or intermittent nature of the flow, predicts asymptotic statistics that depend only on the velocity jump ΔU across the layer. All other details of the initial state are assumed to be wiped out. Such a picture may well be oversimplified, and if so, these turbulent flows could be completely non-universal. Or, in analogy with expectations for the three-dimensional cascade, there could be universal corrections to the simple scaling results as yet, neither measured nor calculated.

To address the problem we have performed a number of numerical simulations of the two-dimensional shear layer using the vortex-in-cell algorithm described by Christiansen (1973). The numerical scheme is discussed in § 2. The coherent structures observed experimentally correspond to islands or blobs of vorticity in two dimensions. The vortex pairing in the mixing layer has as its counterpart the merging or fusion of two or more of these blobs of vorticity. This process constitutes a well-defined event. Extrapolations from experiment suggest that the two-dimensional shear layer will consist at every stage of a linear arrangement of blobs of vorticity. The blobs should merge, mainly by pairing with nearest neighbours, and thus increase in strength, size and mutual separation. The thickness of such a layer is simply related to the size of individual vortex blobs. One has to admit this picture as a logical possibility in the absence of quantitative theory. It was for example assumed by Takaki & Kovasznay (1978) in their kinetic model for the distribution of blob sizes and spacings. However, there are other possibilities. Conceivably the structures once formed could simply scatter more and more about the line on which they originate, leading to an ever thicker layer with merging of two or more structures occurring only through chance encounters. Contour and point plots of vorticity, produced from our simulation and presented in § 3, suggest that some mixture of amalgamation and scatter of vortex blobs takes place. The shear layer consists at every stage of an array of clusters of vortex blobs. Each cluster is a bound state of a few vortex blobs. The size of these clusters, and hence the degree of scatter of the vortex blobs about the midline, determines the layer thickness. The average size of individual islands of vorticity does not scale with the layer thickness, although it does increase in time as vortex islands within a cluster merge.

In § 3 we also present and discuss scaling plots for the profiles of mean velocity, transverse and longitudinal velocity fluctuations, Reynolds stress and the intermittency factor. Some interesting fluctuations in the Reynolds stress as a result of pairing events are displayed. Finally, we discuss the importance of the vortex structures for the processes of entrainment and mixing of a passive marker. This leads us to suggest that flow visualization experiments using a dye may overestimate the size of vortex structures.

In § 4 equilibrium statistical mechanics is applied to the problem of determining the vorticity profile, a question addressed experimentally, in a low-Reynolds-number mixing layer, by Browand & Weidman (1976). Saffman & Baker (1979), extending a train of thought that goes back to Onsager (1949), have conjectured independently that equilibrium statistical mechanics might be relevant to the vorticity distribution within turbulent structures. If the vortices merge at some critical separation, and if they equilibrate between mergings, conservation of energy and angular momentum

suggest that the vortex profile converges to a universal form through successive mergings. All length scales based on a single vortex structure then scale together. If we could assume that at every stage the vortex blobs were simply arranged along a line, the conservation laws alone suggest that the ratio of vortex size to vortex separation locks into a fixed value. These observations are relevant to discussions of the validity of simple scaling. In §4, and again in §6, relationships with the dual cascades of isotropic turbulence in two dimensions (Kraichnan 1967; Batchelor 1969) are pointed out.

We have verified that the results of §3 are insensitive to our level of spatial resolution, truncation errors, residual anisotropy, etc. Consistency checks on the numerical procedures are discussed in §2 and again in §5 along with experimental results for the turbulent mixing layer. We conclude §5 with a numerical study of the propagation of error from small to large scales as the shear layer evolves. This is achieved by comparing two simulations with different spatial resolution. Section 6 contains a summary and outlook.

2. Numerical scheme

A two-dimensional flow field can be represented by an assembly of discrete vortices, and the time evolution of the field transcribed into a particle mechanics of the vortices. With N vortices, a time step in a direct summation scheme will involve evaluating $N - 1$ terms for the velocity of each vortex, and thus on the order of N^2 terms per time-step. For large N such a code will be very time consuming. Thus, the mixing-layer calculation of Ashurst (1977), where the number of vortices was increased from 1 to 800, required 250 hours of computing time on a CDC 6600. Understandably, previous direct summation calculations were much more modest. Michalke (1964) studied the linear and partly nonlinear instability of 72 vortices arranged on three close parallel lines. Acton (1976) studied the same problem, but with 96 vortices arranged initially on four close sinusoids, and ran for a longer time. In Acton's simulation the sinusoid is seen to amplify, break and form two vortex blobs which then fuse into one.

An alternate method for time-stepping vortices was described by Christiansen (1973) (see also Christiansen & Zabusky 1973). In this algorithm the basic variables are still the positions and strengths of the vortices, but now a grid is laid down covering the flow area. At every time-step a grid vorticity is generated by smoothing the vorticity from each vortex onto the four neighbouring grid points. This grid vorticity is then used to generate a grid stream function by solving Poisson's equation. The stream function is differenced on the grid to produce a velocity field, which is finally interpolated back to the vortex positions. The advantage of this apparently rather elaborate detour is, that the Poisson inversion can be accomplished by fast Fourier transform techniques. If the grid is $M \times M$, this is an order $M^2 \log_2 M$ calculation. Since the number of grid squares, M^2 , is some small multiple of the number of vortices N , this requires on the order of $N \log_2 N$ operations per time-step. (The smoothing and interpolations are order N operations). When N is large, $N \log_2 N$ is considerably smaller than N^2 . The method of Christiansen (1973), or cloud-in-cell method as it is sometimes called, is used in this paper with $N = 4096$ and $M = 256$ for the main calculation. In this algorithm the vortices effectively have finite cores, equal in size

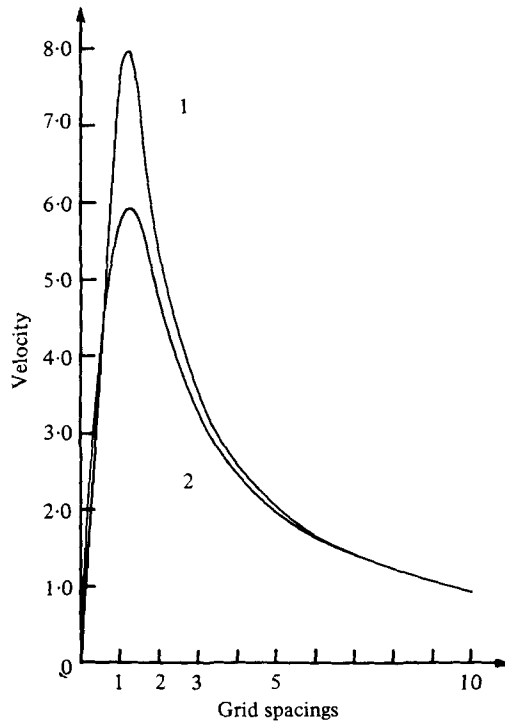


FIGURE 1. Anisotropy of interaction velocity. Curve 1, y velocity along line parallel to x axis. Curve 2, tangential velocity along line at 45° to x axis.

to a grid square. This is an advantage, since it makes the time evolution less singular than it would be for an assembly of point vortices, two of which could come very close. We refer to Zabusky (1977) for a general review of numerical methods used to study structures in turbulent flows. See also Leonard (1980) and the recent 'contour dynamics' approach of Deem & Zabusky (1978) and Zabusky, Hughes & Roberts (1979).

Our basic flow box is a unit square with rigid boundaries at the top ($y = 0.5$) and bottom ($y = -0.5$), periodically continued in the x direction. The initial configuration is a line of identical vortices with $y = 0$, and x between 0 and 1. For the main calculation the vortices are put down randomly along the midline. To obtain a regular roll-up the vortices are uniformly spaced and given a sinusoidal perturbation of the appropriate wavelength. Since a vortex is smoothed over four grid points, and since effects of the periodic boundaries are apparent when the layer has thickened to about one quarter of the flow box width, the number of vortices was chosen as $N = 0.25 \times 0.25 \times M^2$. For $M = 256$ this gives 4096 vortices. Various subsidiary calculations employed a 64×64 grid with 1024 vortices. Putting in more vortices would not improve spatial resolution. All computations were performed on the CRAY-1 computer at the National Center for Atmospheric Research (NCAR).

One pays a price for the computational efficiency of the cloud-in-cell scheme. It turns out, that the interaction of two vortices becomes anisotropic and depends not only on the separation of the vortices, but also on the angle between the separation vector and the axis of the grid: figure 1 illustrates this effect. We placed a vortex at

random within a grid square and calculated the y velocity induced at a series of positions displaced along the x axis. This gave the curve labelled 1 in figure 1. We also calculated the tangential velocity along a line at an angle of 45° with the x -axis. This gave curve 2 in figure 1. The anisotropy is readily apparent. At separations larger than a few grid spacings the velocity is essentially isotropic.

We have dutifully worried about this point. The importance one is willing to attach to it depends on the type of problem under investigation. If the objective is to study the instability of some steady configuration of vortices, we believe, that it is crucial to eliminate the anisotropy. Christiansen (1973) showed, that a system of 3002 vortices, arranged to simulate a disk of uniform vorticity, produced spurious boundary wave modes, although the conservation laws were well maintained. He traced this numerical error of the cloud-in-cell scheme to the velocity anisotropy. Let us anticipate, that our flow will evolve into an arrangement of compact vortex blobs, separated on average by several times their radius and thus many grid spacings. The code will then correctly produce isotropic interaction between blobs. Since it breaks rotational invariance, the anisotropy would tend to make

$$L^2 = (1/N) \sum_{\alpha} r_{\alpha}^2 \quad (2.1)$$

drift in time. Here r_{α} is the distance of vortex α from the centroid of the assembly, and we have assumed all vortices to have the same strength. It was this quantity, that we loosely referred to as the angular momentum in §1. We have checked that L^2 is in fact well conserved for a system of 250 vortices arranged to resemble one of the vortex blobs seen in the simulation. The code also conserves the vortex blob energy. We believe (§4) that preservation of both energy and L^2 guarantees that we will reproduce the correct statistical mechanics for vortex blobs, and this is our main point of concern.

Nevertheless, we have redone several runs with an isotropic interaction velocity-generated by truncating modes at high wavenumber in the Poisson inversion. Fourier components of the stream function were set to zero outside a circle in wavenumber space with radius equal to half the maximum wavenumber fully represented by the chosen grid. This is equivalent to smoothing the vortices over more than the four surrounding grid squares. Buneman (1973) and Hockney, Goel & Eastwood (1974) have considered more elaborate real-space smoothing schemes, and have shown that these will reduce the anisotropy effectively to zero. On a vector machine like the CRAY-1 however, it is more efficient to do the smoothing in wave-vector space using a cut-off. The reason is clearly that the two-dimensional FFT is vectorizable and goes very fast, while the smoothing operations involve a random look-up that does not vectorize and should thus be kept as simple as possible. Our code required about as much time to do the simple four-point smoothing as it needed to do the Poisson inversion. A simulation run with the wavenumber cut-off showed no significant differences from the results reported later in the paper.

Since the most time consuming part of the code is the evaluation of the vortex velocities, it is clearly advantageous to use a time-stepping scheme that takes as large time-steps as possible for a given accuracy. Some initial experimentation convinced us that we would do considerably better with a predictor-corrector method than with the traditional leap-frog scheme. The time-stepping algorithm adopted is the code STEP of Shampine & Gordon (1975).

A cloud-in-cell vortex code does not exactly conserve the grid kinetic energy or the

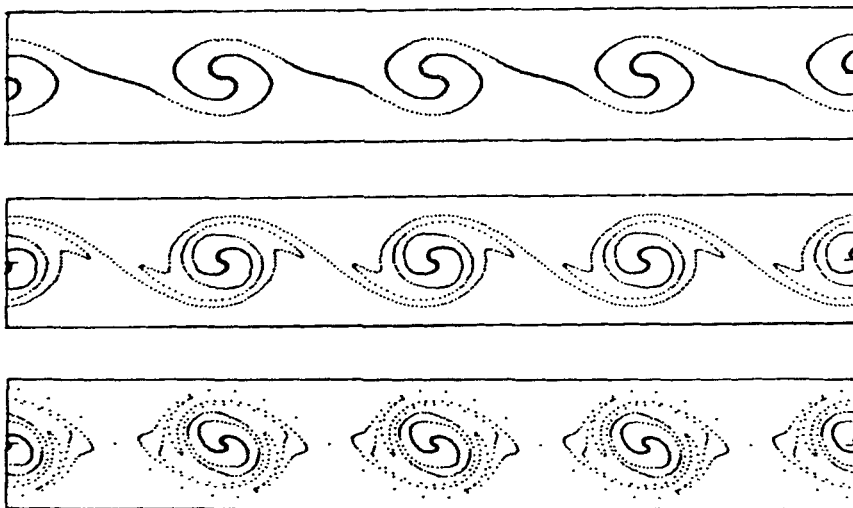


FIGURE 2. Roll-up of a sinusoidally perturbed, regularly spaced line of identical vortices from a run with 4096 vortices on a 64×64 grid. Only half the layer is shown.

grid enstrophy. The former fluctuates randomly (by approximately 0.1 % during the entire simulation), while the latter gradually decays. All circulation integrals around loops larger than about one grid square are conserved however. The gradual decay of enstrophy in the simulation has a natural interpretation. The finite spatial resolution imposed by the grid acts as an eddy damping on the smallest scales, and destroys any enstrophy that reaches these scales. We shall discuss this in more detail in §4. Errors in the integration, from time-stepping inaccuracies or truncation, will tend to act like random noise and thus diffuse vortex blobs. As we shall see, there is very little diffusion, and the blobs are surprisingly compact and stable.

We include in figure 2 a sequence of pictures showing the initial regular stages of roll-up of a vortex sheet. The initial condition used to produce this figure was a line of 4096 vortices regularly spaced and given a sinusoidal perturbation of small amplitude. The underlying grid used was 64×64 . Figure 2 reproduces only half the layer. Perfect periodicity was enhanced by choosing the wavelength of the perturbation to be an integral number of grid spacings. The regular wrapping up of the layer observed is in qualitative agreement with theoretical expectations (cf. Damms & Küchemann 1974). The existence of many regular windings within each rolled up vortex core indicates that truncation and time-stepping errors are indeed well controlled. As the evolution continues, the fine structure in the outer regions of each of the big vortices is obliterated. The central S-shaped feature survives until the first pairing. We have also compared this layer with a run starting from a regular, sinusoidally perturbed line of only 256 vortices, each of which was 16 times as strong as those in the previous run so that the velocity jump across the layer was the same. From contour plots of the grid vorticity at a given value of the layer thickness it is impossible to discern this difference of a factor 16 in the number of vortices used.

3. Results of numerical simulation

The fields of vorticity ζ and velocity (u, v) are known on the points of the grid in our simulation. From these values we can calculate approximate x averages, such as

$$\bar{\zeta}(y, t) = \int_0^1 dx \zeta(x, y, t), \quad (3.1)$$

$$\bar{u}(y, t) = \int_0^1 dx u(x, y, t), \quad (3.2)$$

etc. If we imagine increasing the size of the simulation, the averages $\bar{\zeta}$, \bar{u} , ... must converge. We could equally well reduce fluctuations by averaging over initial conditions.

The mean velocity \bar{u} goes to a constant value, $\frac{1}{2}\Delta U$, well below the shear layer, and to $-\frac{1}{2}\Delta U$ well above it. Thus we can introduce the length

$$\theta(t) = \int dy (0.25 - (\bar{u}/\Delta U)^2) \quad (3.3)$$

as a convenient measure of the layer thickness. There are of course many other measures of shear-layer thickness. The momentum thickness (3.3) was used by Winant & Browand (1974) and by Browand & Weidman (1976).

Asymptotic self-preservation requires, that any other transverse length scale become a fixed multiple of θ as the flow evolves, and that simple scaling should hold. For example, we want to check

$$\overline{u^2} - \bar{u}^2 = (\Delta U)^2 f_{||}(y/\theta), \quad (3.4)$$

$$\bar{v}^2 = (\Delta U)^2 f_{\perp}(y/\theta), \quad (3.5)$$

$$\bar{uv} = (\Delta U)^2 f_{\times}(y/\theta), \quad (3.6)$$

along with (1.1), where the functions $f_{||}$, f_{\perp} , f_{\times} are universal. The thickening rate

$$r = (d\theta/dt)/\Delta U \quad (3.7)$$

should be a universal number. Our simulation gave $r = 0.02$ with an uncertainty of about 30 % (cf. figure 3). This value is consistent with experimental values for the mixing layer (Browand & Latigo 1979). The obvious transcription from temporal to downstream evolution gives $d\theta/dx = 2r\Lambda$ for the mixing-layer growth rate, where r is given by (3.7).

In the simulation $\theta(t)$ was calculated at each time-step. The variation of θ with time is shown in figure 3. Roughly, θ grows linearly with time. The momentum thickness θ does not vanish at $t = 0$ owing to the finite spatial resolution imposed by the grid. The initial growth of θ in a real fluid is not linear in time but proportional to $(\nu t)^{\frac{1}{2}}$ where ν is the kinematic viscosity. As the layer thickens and Reynolds number increases a cross-over to linear growth occurs. This happens early in our simulation because of the very small amount of dissipation. The wiggles in $\theta(t)$ reflect that the layer thickens through interactions among large vortex structures. The number of these macrovortices captured in our simulation is at most 30–40 and decreases as the layer thickens. The wiggles in $\theta(t)$ are statistical fluctuations due to the finite size of the simulation.

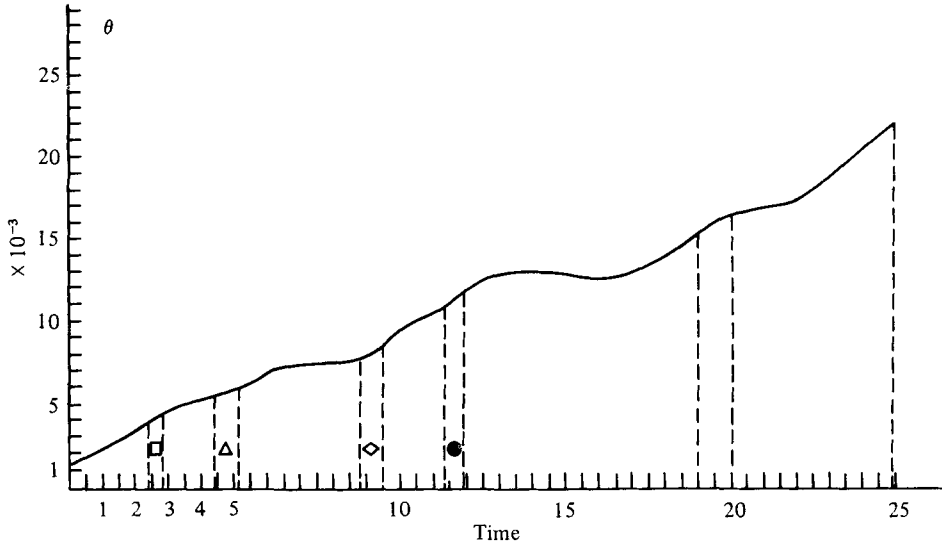


FIGURE 3. Variation of the momentum thickness, $\theta(t)$, for our principal calculation with 4096 vortices on a 256×256 grid. The dimensionless growth rate r , (3.7), equals 0.02. The pairs of dashed lines delimit time intervals over which the x -averaged velocity profiles were time averaged. The symbols correspond to those in figures 11–14.

This is discussed further under (e). We believe that in an ensemble average of runs the wiggles would be eliminated. The simulation was terminated when about 8 large vortex structures remained. This is comparable to the state at which previous numerical work began.

Several dashed lines appear in figure 3, all except one are in pairs and the first four pairs have a symbol drawn in between. The left line of each pair and the single line at $t = 24.9$ correspond to values of θ given by $256 \times \theta = 1, \sqrt{2}, 2, 2\sqrt{2}, 4, 4\sqrt{2}$, respectively. Vorticity plots corresponding to these values of θ appear in figures 4, 5, 6 and 7. At each of these values of θ a time average of profiles, scaled by the current value of $\theta(t)$, was initiated. The time average ran from the left-hand to the right-hand dashed line in each pair. The momentum thickness θ increased by about 10% during each time averaging. The time-step, which was variable, was recorded and used to weight the terms in the average. A variance was also calculated to assess the magnitude of fluctuations. Scaled, time-averaged profiles corresponding to different states of evolution of the shear layer are shown in figures 10–14. The symbols used in figures 11–14 correspond to the symbols in figure 3. The reader should have little trouble cross-referencing the figures. We now discuss the results in turn.

(a) Flow visualization

Figures 4 and 5 show point plots of vorticity for the left half of the shear layer at selected values of θ . Only a band down the middle of the 256×256 grid is shown. There was no vorticity outside the band shown. Figures 6 and 7 show contour plots of one-fourth of the shear layer, again displayed to bring out the time evolution. It is clear from these pictures, that the shear layer has already rolled up into discrete vortices at $\theta = 1/256$, and that the dynamics of these structures dominates the

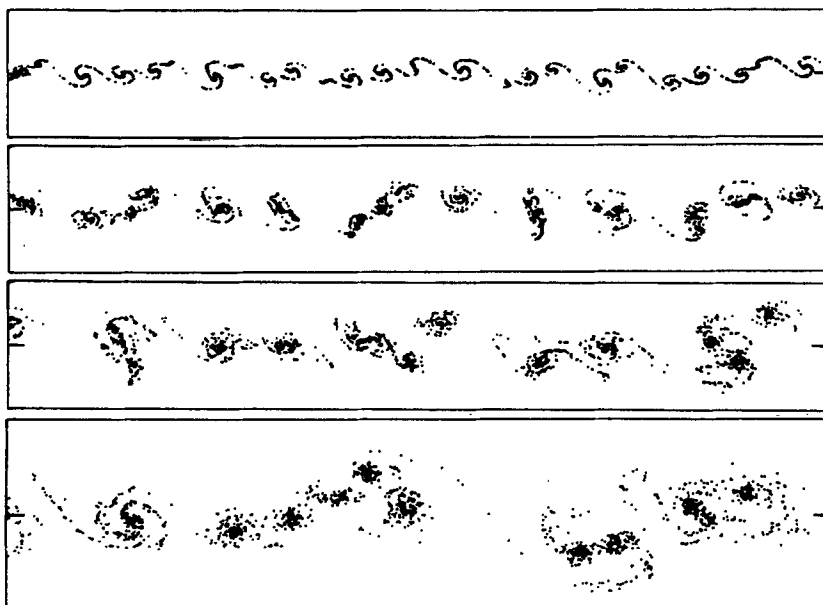


FIGURE 4. Point plot of vortices, for one half of the simulated layer, $0 < x < 0.5$. θ increases from top to bottom such that $256 \times \theta = 0.64, 1, \sqrt{2}, 2$ lattice spacings.

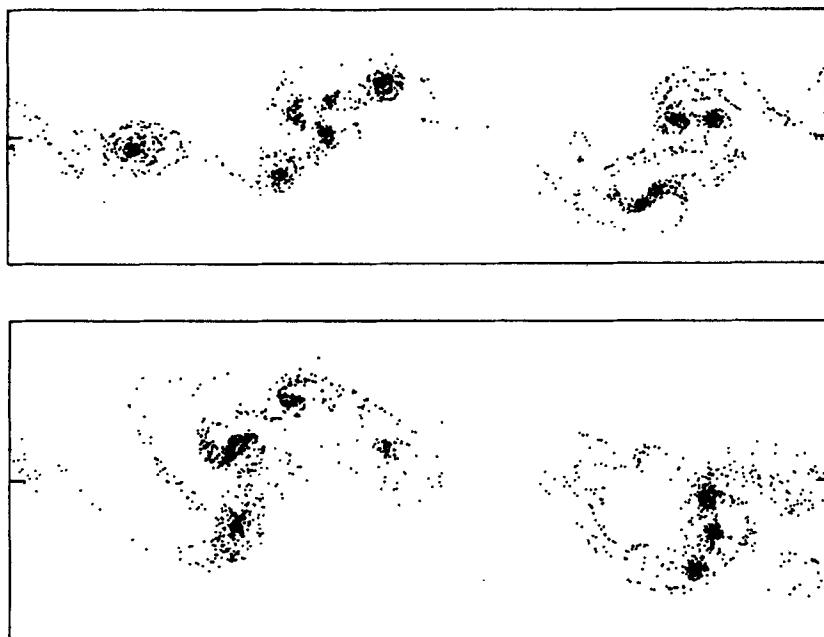


FIGURE 5. Continuation of figure 4 for $256 \times \theta = 2\sqrt{2}$ (top), 4 (bottom).

evolution. The plots show that the macro-vortices have a peaked distribution of vorticity, and that they are well separated with a lot of irrotational fluid in between. This is a very different conceptual picture of the shear layer than the traditional band of random vorticity implicit in most discussions that start from Reynolds' equations.

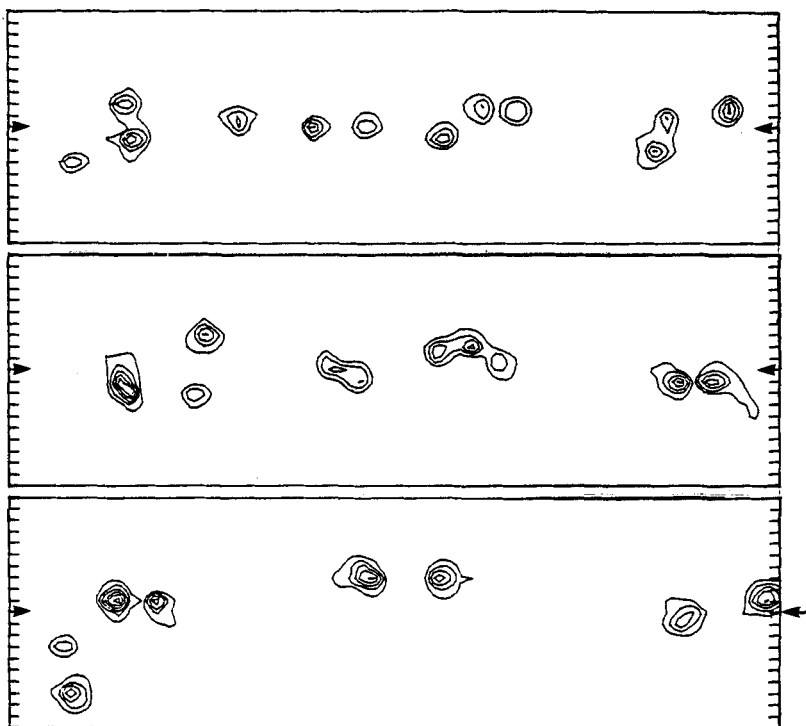


FIGURE 6. Contour plots of vorticity for one quarter of the simulated layer, $0.75 < x < 1.0$, with θ increasing top to bottom: $256 \times \theta = 1, \sqrt{2}, 2$. The small arrows indicate the centre-line. The grid vorticity divided by its maximum has been contoured using the same levels in each panel.

In figures 6 and 7 the grid vorticity $\zeta(x, y, t)$ normalized by its maximum value $\zeta_{\max}(t)$ has been contoured using a fixed set of contour levels for all times. (We are indebted to F. K. Browand for suggesting this way of displaying the data). The layer thickness θ increases by a factor of $\sqrt{2}$ from one panel to the next in figures 6 and 7. If the vortex blobs scale it should be possible to obtain one panel from the previous one (in an average sense) by multiplying all lengths by $\sqrt{2}$. This is clearly not the case in our figures. The individual vortex structures do not grow nearly fast enough. To make this point quantitatively, we calculated short time averages of

$$I_1(r) = \int dx \int dy \zeta(x, y, t) \zeta(x+r, y, t) \quad (3.8)$$

and

$$I_2(r) = \int dx \int dy \zeta(x, y, t) \zeta(x, y+r, t) \quad (3.9)$$

for $r = 0, 1, \dots, 30$ grid spacings. Normalizing by the lattice enstrophy, we get the correlation coefficients. These drop very rapidly from their maximum of unity. The widths of the correlation at half maximum are summarized in table 1. Although the widths do increase, it is clear, that they do not scale with θ . Equivalently, the scaling form that one would write down for the correlations on the basis of self-preservation theory is not verified. According to table 1 the vortex blobs are initially a bit elongated in the x direction as one would expect. However, when $\theta \times 256 = 4$ the vortex structures have become circular to within statistical fluctuations.

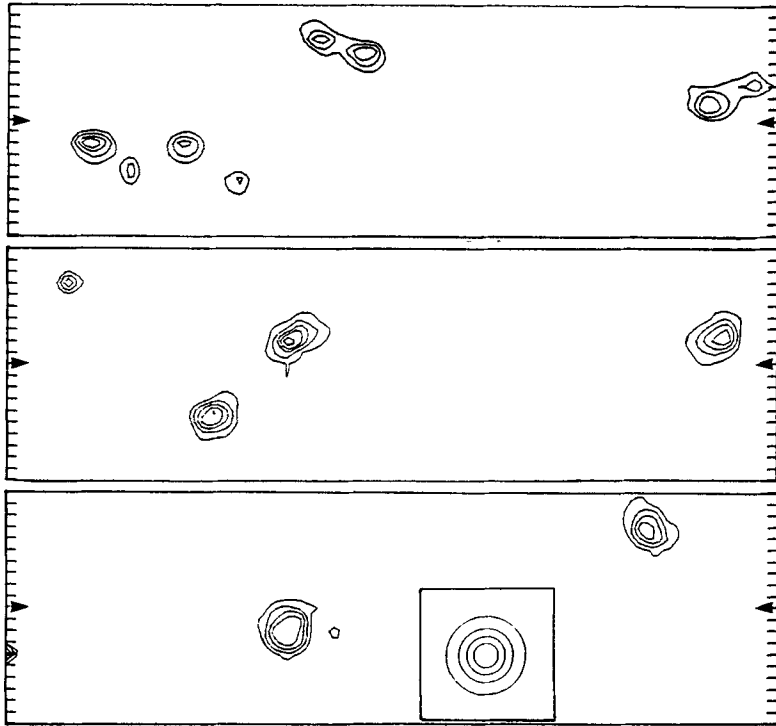


FIGURE 7. Continuation of figure 6 for $256 \times \theta = 2\sqrt{2}, 4, 4\sqrt{2}$. The insert shows the vorticity profile from equilibrium statistical mechanics (§4).

$\theta \times 256$	1	$\sqrt{2}$	2	$2\sqrt{2}$	4
x offset	1.26	1.42	1.58	1.65	1.77
y offset	1.16	1.30	1.34	1.49	1.80

TABLE 1. Widths, in grid spacings, of x -offset and y -offset vorticity correlation coefficients as function of θ .

The pictures in figures 4–7 suggest that the vortices scatter more and more about the midline as θ increases. To check this, the positions of the large vortices were found every 5 time-steps. From their transverse co-ordinates we calculated the average $\langle |Y| \rangle$ of the absolute values and the variance $\langle Y^2 \rangle^{\frac{1}{2}}$. (The average $\langle Y \rangle$ was always close to 0.) In figure 8 we show $\langle Y^2 \rangle^{\frac{1}{2}}/\theta$ as a function of θ . We see that this ratio quickly settles down to a value close to 1.75. The distribution of these macro-vortex co-ordinates apparently also quickly relaxes to a fixed form. This is seen in figure 9 where $\langle Y^2 \rangle^{\frac{1}{2}}/\langle |Y| \rangle$ is plotted versus θ . The average value of $\langle Y^2 \rangle^{\frac{1}{2}}/\langle |Y| \rangle$ is 1.25. If Y were Gaussianly distributed this ratio would be $(\frac{1}{2}\pi)^{\frac{1}{2}} \cong 1.253$.

We also calculated the Fourier transform of vorticity integrated across the shear layer, i.e.

$$z(k) = \int_0^1 dx \exp(-ikx) \int dy \zeta(x, y, t). \tag{3.10}$$

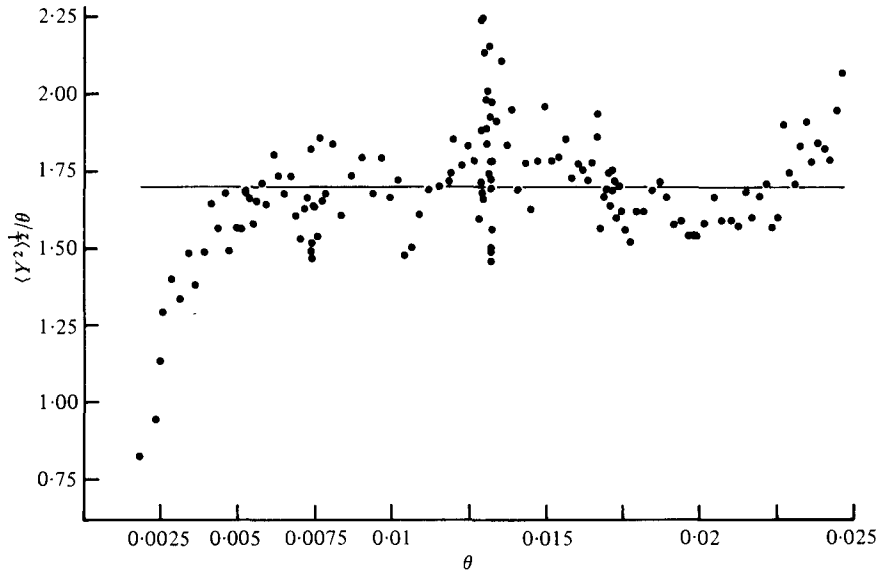


FIGURE 8. Scatter of vortex blob centres as a function of θ . The line marks the average value of $\langle Y^2 \rangle^{1/2} / \theta$.

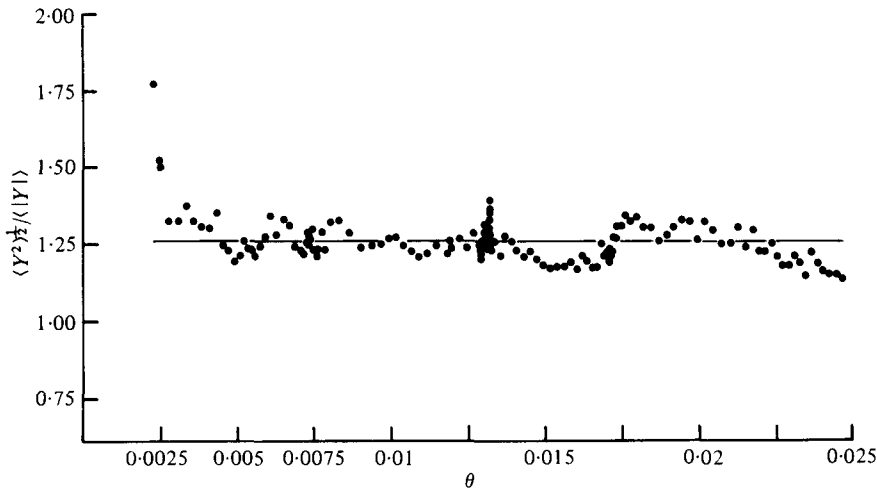


FIGURE 9. Relaxation of the scatter of vortices to a fixed limiting form. The line marks the average value of $\langle Y^2 \rangle^{1/2} / \langle |Y| \rangle$.

The spectrum of amplitudes $|z(k)|^2/|z(0)|^2$ displays the distribution of excitation at various length scales along the layer. As expected the wavenumber of maximum amplitude moves towards $k = 0$ as the layer evolves. This implies that the real space distribution of vorticity along the layer becomes lumpy on a coarser and coarser scale as the layer thickens. This lumpiness is not associated with large vortex regions that span the width of the layer, but rather with clusters of smaller blobs (see figures 4–7). A cluster is a bound state of several distinct islands of vorticity. The bottom panel in figure 6 for example shows a cluster with four vortex blobs

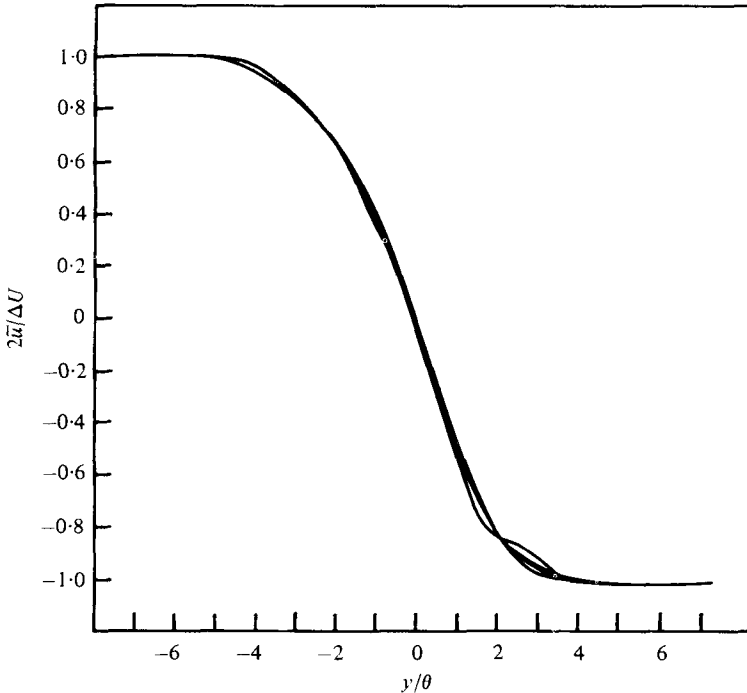


FIGURE 10. Scaling of mean velocity profiles. The scaled profiles at four values of θ , $256 \times \theta = 1, \sqrt{2}, 2, 2\sqrt{2}$, are superimposed.

and two clusters with only two blobs each. A cluster will be surrounded by a closed streamline.

Thus, putting these observations together, we do not see a linear arrangement of vortex structures that merge with neighbours and thus grow in size, but rather a more complex sequence of events. Our vortex structures generally first form bound clusters (figures 4-7), within which the probability of a close encounter leading to vortex merging is enhanced. The clusters, however, can cluster again before a complete merging of the vortices within them has taken place. The size of individual vortex structures thus lags behind the simple scaling prediction. The layer still thickens linearly in time, at least approximately, since the degree of dispersion or scatter of vortex structures about the midline, and hence the size of the clusters, increases linearly with time.

If we consider the shear layer as a line of clusters of vortex blobs, each cluster having a radius S (the radius of the bounding streamline say) that scales with θ , and if we assume that the location of a blob within a cluster is uniformly distributed, i.e. the blob can be anywhere within the disk with equal probability, then it is easy to calculate, that the probability $P(Y)dY$ of finding a blob center within the band $Y - \frac{1}{2}dY < y < Y + \frac{1}{2}dY$ is given by

$$P(Y)dY = (2/\pi)(1 - (Y/S)^2)^{\frac{1}{2}}d(Y/S). \tag{3.11}$$

For such a distribution $\langle Y^2 \rangle^{\frac{1}{2}} / \langle |Y| \rangle = \frac{3}{8}\pi \approx 1.18$.

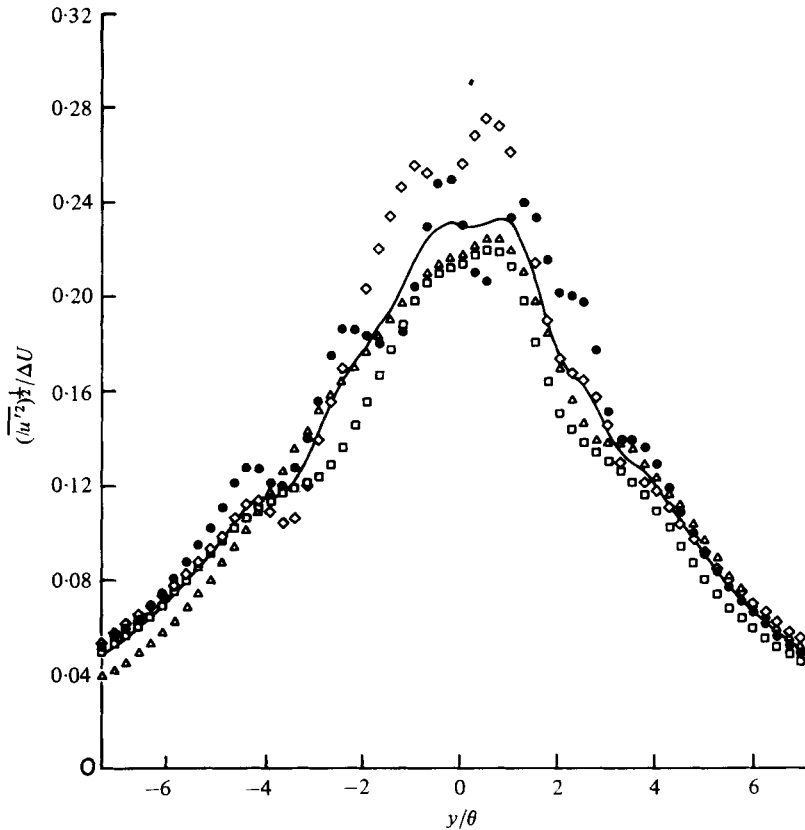


FIGURE 11. Scaling of longitudinal velocity fluctuations. The symbols correspond to those in figure 3.

(b) *Mean velocity profiles*

Superimposing the four earliest time averaged mean velocity profiles yields figure 10. Since the profiles are virtually identical, we have not tried to distinguish them. Scaling of the mean profile is not a very sensitive test of self-preservation.

(c) *Velocity fluctuations*

Figures 11 and 12 test the scaling relations (3.4) and (3.5). The continuous line in these and later point plots represents a simple average of the four sets of data and is only intended to help guide the eye. Although the data do show some scatter, there is no systematic violation of (3.4) or (3.5). Better scaling could be obtained by doing a longer-time average, or doing an ensemble average over several simulations (which is costly in computer time). It is of interest to note that the peak values of the u and v fluctuations, normalized by ΔU , are about 0.25 and 0.30 respectively.

(d) *Intermittency factor*

We define the function

$$I(x, y, t) = \begin{cases} 1 & \text{if } \zeta(x, y, t) > 0, \\ 0 & \text{if } \zeta(x, y, t) = 0, \end{cases} \quad (3.12)$$

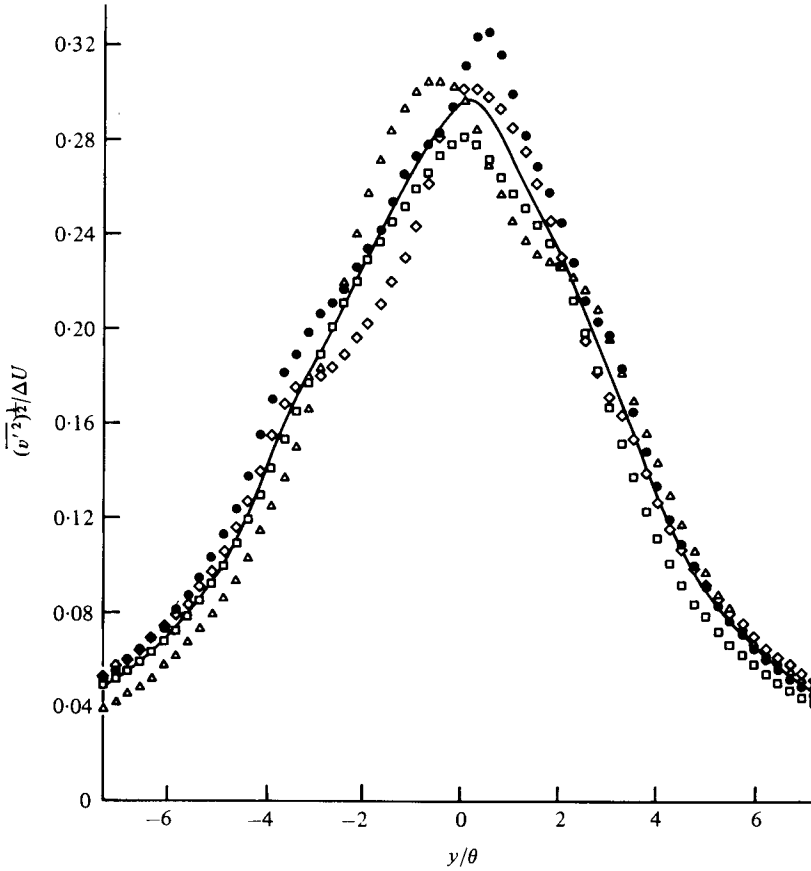


FIGURE 12. Scaling of transverse velocity fluctuations. The symbols correspond to those in figure 3.

and from it the intermittency factor

$$\gamma = \int_0^1 dx I(x, y, t). \quad (3.13)$$

In the simulation the test $\zeta > 0$ was replaced by $\zeta > q$, where q is a small fraction of the strength of an elementary vortex. The values of γ did not change when q was decreased by a factor 100.

The scaling form for γ is simply

$$\gamma = g(y/\theta), \quad (3.14)$$

and figure 13 checks this relation. It is noteworthy, that γ drops to about 0.65 on the axis. The low peak value of γ is consistent with the well separated vortices, but figures 6–7 would have suggested even smaller values for γ . There are however non-negligible regions of low vorticity suppressed by the finite number of contour levels used in these figures but apparent in figures 4–5. This ‘debris’ arises during the merging of vortices (cf. Christiansen 1973) and can also occur if a vortex is torn apart in the shear field of its neighbours (Moore & Saffman 1975) although we have not actually seen this

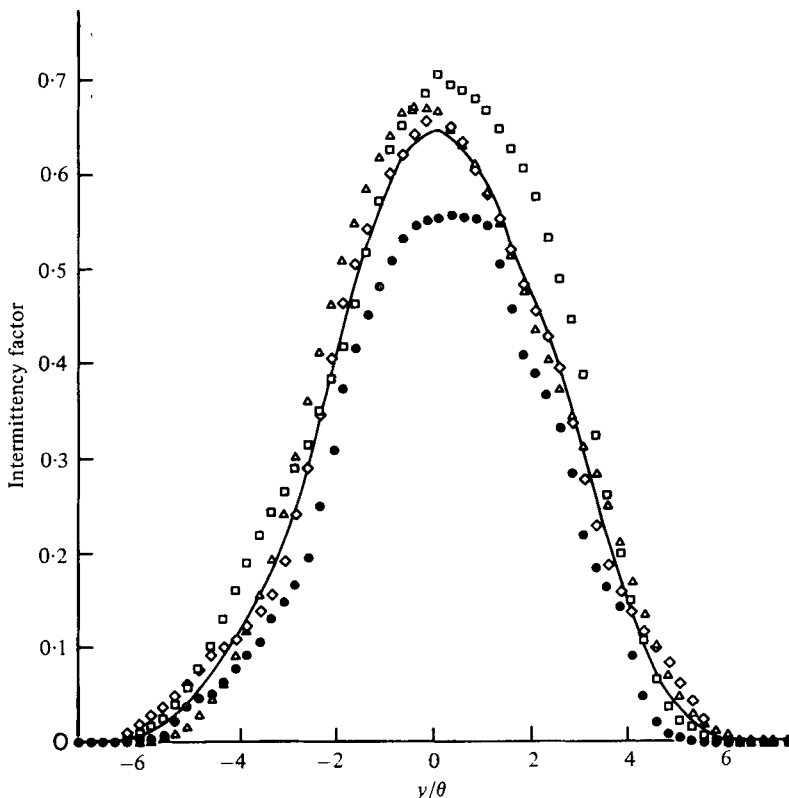


FIGURE 13. Scaling of intermittency factor. The symbols correspond to those in figures 3, 11 and 12.

happen. It is an open question whether the vortex structures will persist or whether they will very gradually diffuse away into a slowly increasing background of distributed vorticity.

(e) *Reynolds stress*

The scaling given by (3.6) is not satisfied at all well in our simulation as figure 14 shows. We do not think of this as a systematic deviation but simply as the result of large statistical fluctuations in a small sample. To show this more clearly, we considered a very simple flow with only four large vortices. These were generated by superimposing a sinusoidal wave, of the appropriate wavelength, on an initial, regularly spaced line of vortices. As the four vortices paired, we monitored the Reynolds stress. Figures 15(a, b, c) show three of the results together with the vortex configurations that produced them. Because of cancellations due to fluctuations in sign of uv , apparent in figures 15, one needs better statistics on this quantity than on the longitudinal and transverse velocity fluctuations which are positive definite quantities. In a large system, \overline{uv} is a sum of contributions from pairs in various stages of relative rotation or amalgamation, and a much longer layer than ours (or an ensemble average) is necessary to produce smooth averages.

The statistical fluctuations discussed here are related to the wiggles in the $\theta(t)$ graph

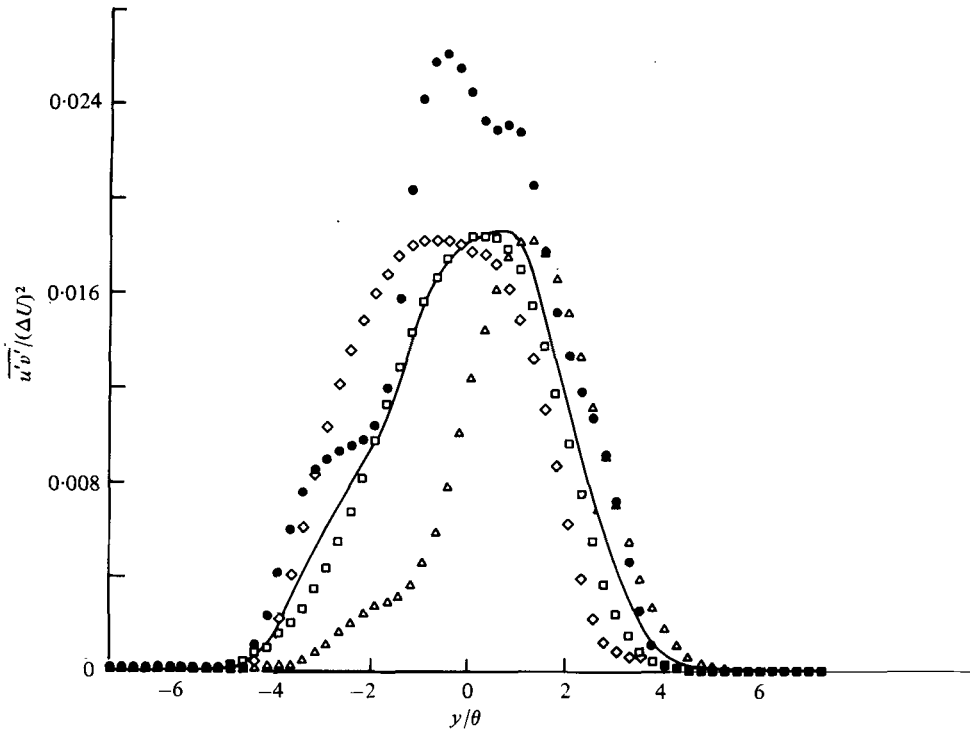


FIGURE 14. Test of Reynolds' stress scaling. The symbols correspond to those of figure 3.

in figure 3. To see this we note the formula

$$\dot{\theta} = 2 \int dy \bar{\xi} \overline{uv} / (\Delta U)^2, \tag{3.15}$$

where $\bar{\xi}$, \overline{uv} are x averages as in (3.1), (3.2). Equation (3.15), which is derived in an appendix, follows simply from the definition (3.3) of θ and the two-dimensional Euler equations. Since $\bar{\xi}$ is always positive, θ will grow as long as \overline{uv} is positive. Negative excursions of \overline{uv} will impede the growth of θ .

For these reasons the earlier computations of Acton (1976), containing only two large vortices, were insufficient to say much about the shear-layer problem.

(f) *Entrainment and mixing*

Figures 16(a, b, c) give some qualitative insights into the interaction between the vortex structures and a passive marker during the process of entrainment and mixing, a problem studied experimentally by Dimotakis & Brown (1976). A line of 512 markers was introduced well above the vortices. Figures 16(a, b, c) show that the markers were quickly pulled in between the vortices. Some of the markers appear below the shear layer after one period of rotation of the large vortices. Small-scale structure in the marker density is quickly created. The markers really never enter the regions of high vorticity but are continually stirred as the vortices move about. Hence the coalescence of vortices seems to play only a minor part in the mixing.

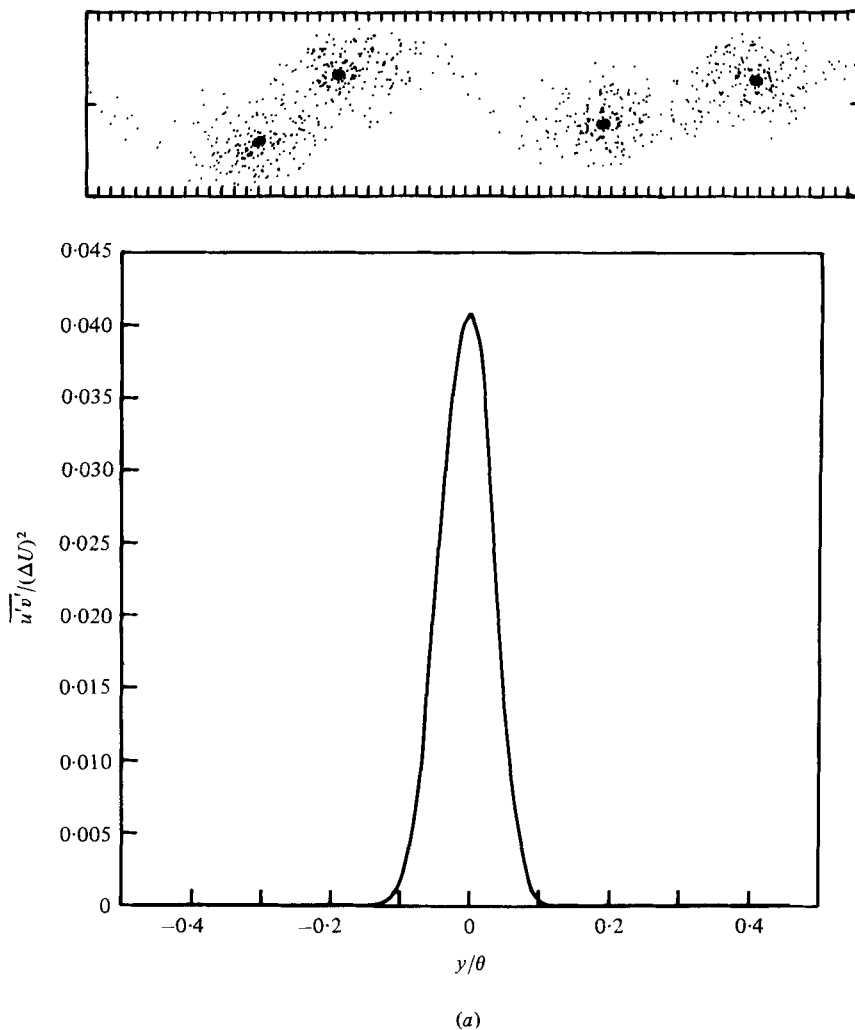


FIGURE 15 (a) for legend see page 726.

An intermittent distribution of vorticity is crucial if the two-dimensional shear layer is to mix a passive scalar efficiently. In the absence of viscosity

$$D\xi/Dt = 0 \quad (3.16)$$

is the equation of motion of vorticity, and in the absence of diffusion

$$Ds/Dt = 0 \quad (3.17)$$

governs the evolution of the scalar density s ; D/Dt is the material derivative. Thus for every realization

$$D\xi s/Dt = 0 \quad (3.18)$$

in this limit. Now if the vorticity always occupied a uniform band (with the intermittency factor equal to unity on the centre-line), only diffusive effects would allow scalar starting above the layer to be mixed with scalar below. This process differs in

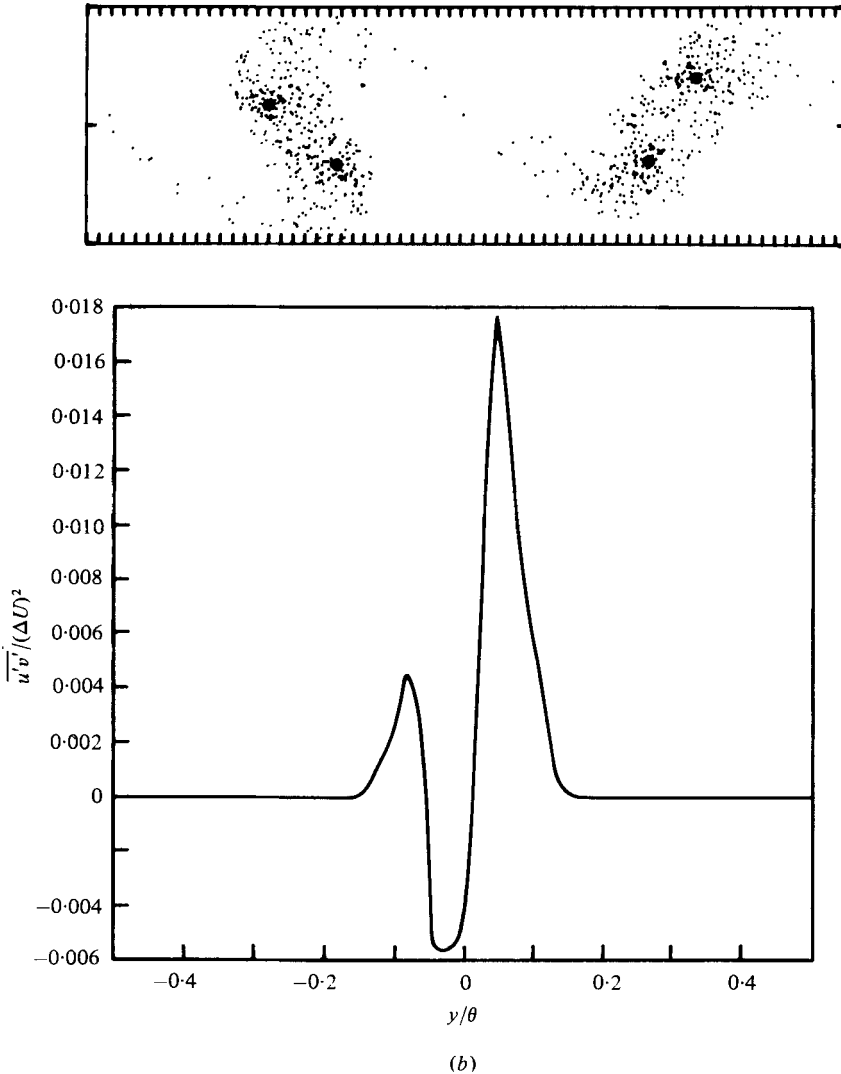


FIGURE 15 (b). For legend see page 726.

essential ways from the entrainment by large structures that actually occurs. Diffusive mixing is almost entirely inhibited in our simulation, yet transport of scalar across the shear layer takes place in one large eddy turnover time due to the existence of an intermittent distribution of vortex structures.

Figure 16(c) shows the marker thoroughly mixed. Had we not shown the vorticity distribution along with the markers in this picture, it would have been very difficult to guess even the number of discrete vortex blobs. The overall distribution of marker would suggest just one large vortex in figure 16(c). This point is worth keeping in mind when interpreting flow visualization experiments. The vortices producing a given dye pattern could be much more compact than the distribution of dye would suggest. The clusters of vortex blobs observed in the later stages of our simulation would probably appear as single structures in a dye experiment.

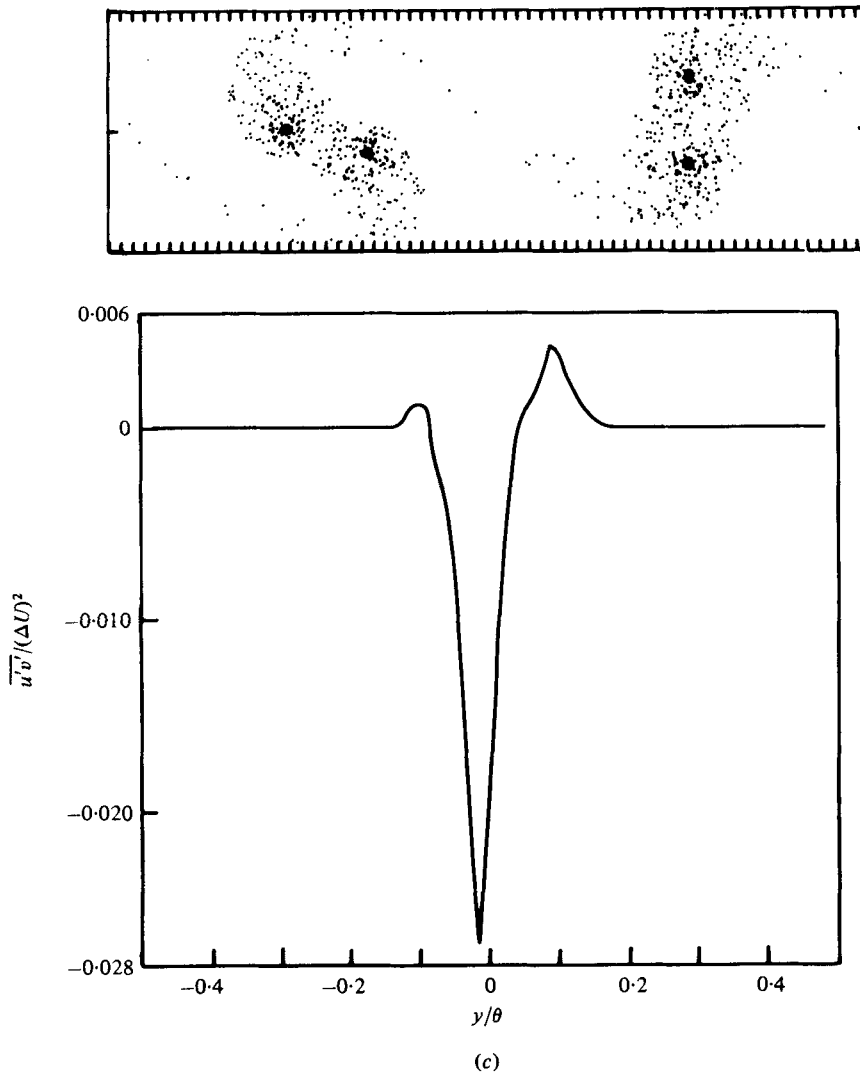


FIGURE 15. Three instantaneous views of the Reynolds' stress and vorticity distribution during vortex pairing.

4. Statistical mechanics of vortices

Two finite area vortices will rotate around one another and merge on a time scale no shorter than R^2/Γ , where Γ is the total circulation of one vortex and R is their separation. On the other hand, the time scale for internal motions within each vortex is of the order L^2/Γ , where L^2 was defined in (2.1). If $R \gg L$ one expects that the individual vortices will equilibrate between mergings. The inequality $R > L$ is definitely satisfied in our simulation, and we are led to suggest that the vorticity profile of any individual vortex blob should be calculable from equilibrium statistical mechanics. The problem of finding the equilibrium distribution of an isolated system of identical point vortices, making up a finite area vortex, has been considered by Kida (1975) and by Lundgren & Pointin (1977).

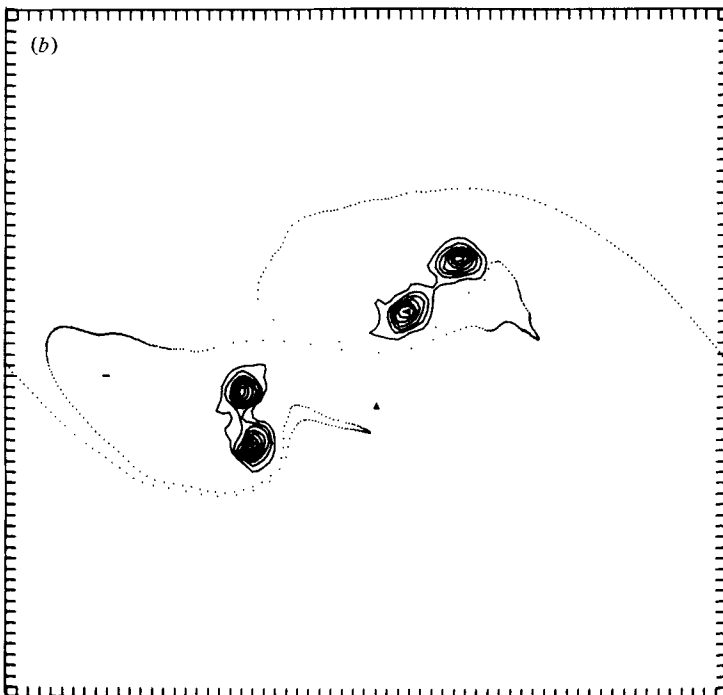
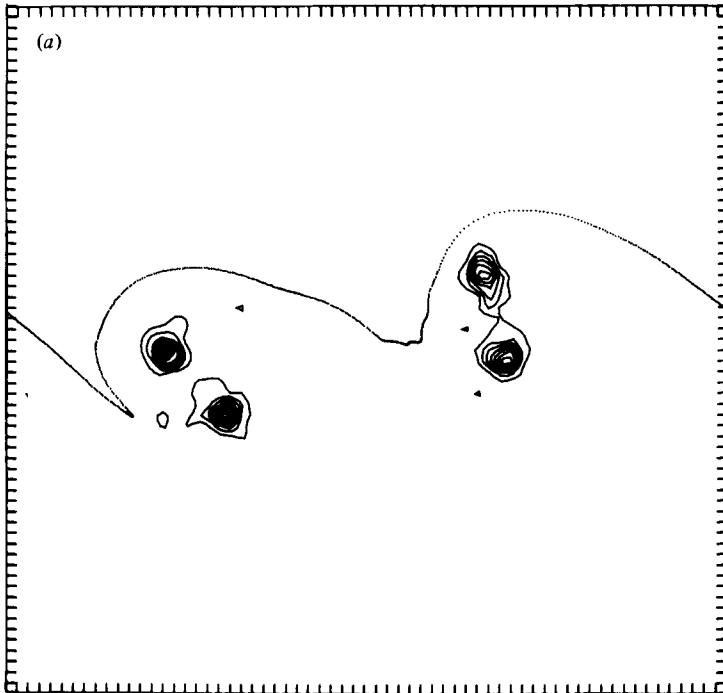


FIGURE 16 (*a*, *b*) for legend see page 728.

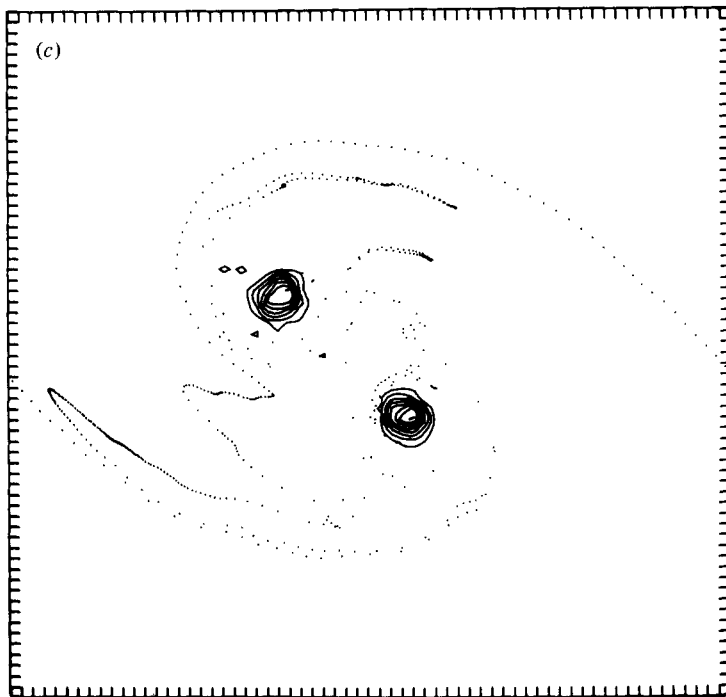


FIGURE 16. Entrainment and mixing of passive marker. The vorticity has been contoured and the markers are shown as points.

In the notation of the second paper, the basic variable is the overall vorticity profile,

$$\zeta(\mathbf{r}) = (\Gamma/L^2) P(\mathbf{r}/L), \quad (4.1)$$

which is determined from an integral equation for the function P ,

$$P(\boldsymbol{\eta}) = C \exp \left[-(1+\lambda) \eta^2 + 4\lambda \int d\boldsymbol{\eta}' \ln |\boldsymbol{\eta} - \boldsymbol{\eta}'| P(\boldsymbol{\eta}') \right]. \quad (4.2)$$

The constant C is determined such that

$$\int d\boldsymbol{\eta} P(\boldsymbol{\eta}) = 1. \quad (4.3)$$

Equation (4.2) is simply an integrated form of the Poisson equation for the stream function, where the vorticity has been evaluated in a canonical ensemble based on conservation of energy and L^2 . In linearized form, and neglecting the angular momentum L^2 , (4.2) reduces to the familiar Debye-Hückel theory of a plasma (Landau & Lifshitz 1969). There is a one parameter family of equilibria distinguished by the value of the parameter λ , $-1 < \lambda < \infty$. It follows from (4.2) and (4.3) that

$$\int d\boldsymbol{\eta} \eta^2 P(\boldsymbol{\eta}) = 1, \quad (4.4)$$

i.e. that the L^2 appearing in (4.1) is given by (2.1). Here Γ is the total circulation of the finite area vortex. The energy of the vortex is

$$E = \Gamma^2 (\tilde{E}(\lambda) - (1/4\pi) \ln(L/l_0)), \quad (4.5)$$

where l_0 sets the scale of length and

$$\tilde{E}(\lambda) = (-1/4\pi) \int d\boldsymbol{\eta} \int d\boldsymbol{\eta}' \ln |\boldsymbol{\eta} - \boldsymbol{\eta}'| P(\boldsymbol{\eta}) P(\boldsymbol{\eta}'). \quad (4.6)$$

With P determined from (4.2), the function $\tilde{E}(\lambda)$ is a monotone decreasing, convex function of λ that goes to infinity as $\lambda \rightarrow -1$, and to a fixed value as $\lambda \rightarrow \infty$. In the infinite λ limit the vortex blob is just a uniform disk of constant vorticity. For $\lambda = 0$, $P(\boldsymbol{\eta})$ is a two-dimensional Gaussian as is seen directly from (4.2). As $\lambda \rightarrow -1$ the vorticity profile becomes more and more peaked. For a given λ the integral equation (4.2) can be solved numerically by iteration. The reader is referred to the papers cited for further details.

We shall assume that this distribution, (4.1), gives the vorticity field $\zeta(r)$ within one of the macro-vortices produced in our simulation and ignores fluctuations due to the finite number of point vortices that form such a structure. In figures 4–7 the number of elementary vortices making up a single large vortex increases from approximately 100 to 500 during the course of the calculation. Let us also ignore differences between the one point approximation and the exact distribution, and ask whether for the two-dimensional shear-layer problem we are using the correct ensemble. Should we, for example, have chosen an ensemble consistent with enstrophy conservation? This question did not arise in the work of Kida (1975) or Lundgren & Pointin (1977), since they start with an assembly of a large but finite number, N , of point vortices. Any invariant of the Euler equations which is some function of the vorticity (although it may be formally infinite for point vortices) is then taken into account at every step of the calculation by keeping the number of vortices and their strengths fixed. However in the final results the limit $N \rightarrow \infty$ is taken and this destroys conservation of enstrophy. Indeed, if we start with two well-separated equilibrium vortex blobs, let them merge and conserve E and L^2 , the distribution of vorticity in the final equilibrated blob can be calculated using Lundgren & Pointin's (1977) theory. The enstrophy thus calculated will in general be smaller after merging than before. This, we argue, is physically correct.

In the continuum fluid, with a small but finite viscosity, two merging vortices will wrap around each other, and vortex fluid will get drawn out into long, thin filaments. Eventually viscous effects will dominate in these filaments, no matter how small the viscosity is, and enstrophy will be destroyed. This is similar to the traditional picture of an enstrophy cascade (Kraichnan 1967; Batchelor 1969), but with the important difference that here the vorticity is all of one sign, and the cascade turns on as the vortex structures merge, but is turned off within a single equilibrated blob. The value of the enstrophy of a vortex blob in this picture simply adjusts to what it must be in equilibrium for given values of E and L^2 . In somewhat different terms, the back transfer of energy that accompanies the usual enstrophy cascade is inhibited by the conservation of L^2 . In our numerical simulation we do not have a real viscosity, but the finite spatial resolution of the grid destroys enstrophy that reaches the smallest scales. From runs with only a few vortex blobs we have numerical evidence that the lattice enstrophy decreases when a vortex merger goes to completion.

Although each vortex blob in the shear layer is deformed by the velocity field due to all the others, the vorticity plots in figures 4–7 and the data in table 1 show the blobs to be approximately circular on average, and so we shall ignore the deformation in the following arguments.

We now consider the merging of two vortex blobs more quantitatively. Assume for simplicity that they both have the same circulation Γ , the same L^2 relative to their centres and the same value of λ . This configuration should ultimately equilibrate and end up as one vortex blob with a circulation $\Gamma' = 2\Gamma$, and new values L'^2 and λ' of the other two parameters. For large initial separations R , i.e. $R/L \gg 1$, this is a slow process which will involve the diffusive growth of each blob due to the action of the rapid internal motions in the other (Lundgren & Pointin 1977). However, if R is less than some critical separation R_c , which will depend on λ and L^2 , convective merging takes place on a time scale R^2/Γ (Christiansen 1973; Rossow 1977). The function $R_c = R_c(\lambda, L^2)$ can be determined numerically. For example, using 72 vortices arranged initially to simulate two uniform blobs, Rossow (1977) found $R_c(\infty, L^2) = 4.65L$. In any case, the new single blob has

$$L'^2 = L^2 + 0.25R^2 \quad (4.7)$$

by conservation of L^2 for the total system, and application of the parallel axis theorem. By conservation of energy,

$$2\tilde{E}(\lambda') = \tilde{E}(\lambda) + (1/4\pi) \ln(L'^2/LR). \quad (4.8)$$

In equation (4.8) the dependence on R comes from the interaction energy of the two initial, circular vortex blobs, and the arbitrary scale l_0 has dropped out as it should.

It follows from (4.7) that $L'^2 > LR$, and thus from (4.8) that $\tilde{E}(\lambda') > 0.5\tilde{E}(\lambda)$. Hence if $\tilde{E}(\lambda)$ is negative λ' must be less than λ , and the resulting single vortex must be more concentrated than its ancestors. This argument suggests that the vortices in the shear layer, which initially do not have a very peaked vorticity profile, become more and more concentrated through the merging process, at least during the first few merging events.

Now consider only the fast convective merging of close blobs, ignore the eventual diffusive merging of more distant blobs, and thus assume that all merging events occur when $R = R_c(\lambda, L^2)$. If λ quickly converges to an asymptotic value λ^* through successive mergings, R_c becomes simply a multiple of L

$$R_c(\lambda^*, L^2) = fL, \quad (4.9)$$

where f is a pure number. Substituting $R = R_c = fL$ in (4.7), the ratio L'^2/LR may be re-expressed in terms of f . Substituting this into (4.8) and setting $\lambda' = \lambda = \lambda^*$, we get

$$\tilde{E}(\lambda^*) = -(1/4\pi) \ln(f/(1 + 0.25f^2)). \quad (4.10)$$

Equations (4.9) and (4.10) in principle determine the asymptotic parameters λ^* and f .

We can further sharpen our results for the asymptotic blob profile in the hypothetical situation where all the blobs remain collinear. This contradicts our numerical results, but it is interesting to follow through since it indicates how through successive pairings random initial length scales can lock into a universal ratio. A single length scale remains, and scaling as in (1.1), (3.4)–(3.6) follows. We use only the conservation laws to derive the locking. The complicated dynamical information implicit in the function $R_c(\lambda, L^2)$ is not needed.

Consider then a line of equilibrium vortex blobs, all of the same circulation Γ_n , the same size L_n and with separation R_n . The index n refers to the generation. Assume

the vortices merge, roughly in phase along the line, to yield the $n + 1$ 'st generation blobs characterized by Γ_{n+1} , L_{n+1} , R_{n+1} , and so on. The theory must establish recursion formulae that enable one to calculate Γ_{n+1} , L_{n+1} , R_{n+1} given Γ_n , L_n , R_n . In this model the layer thickness θ is proportional to the blob size L .

Assume that on the average b blobs of generation n merge to one blob of generation $n + 1$. Then, by conservation of vorticity

$$\Gamma_{n+1} = b\Gamma_n, \tag{4.11}$$

and since the velocity jump ΔU remains constant

$$\Gamma_{n+1}/R_{n+1} = \Gamma_n/R_n, \tag{4.12}$$

thus

$$R_{n+1} = bR_n. \tag{4.13}$$

Finally, by using the parallel axis theorem the conservation of L^2 when b blobs on a line merge to one requires

$$L_{n+1}^2 = L_n^2 + (b^2 - 1) R_n^2/12. \tag{4.14}$$

Equations (4.11), (4.13), (4.14) provide the desired recursion relations.

It is easy to solve (4.13) and (4.14) together. One finds that regardless of the initial values L_1 and $R_1 (> 0)$, and regardless of the value of $b (> 1)$, the solution will always asymptotically approach

$$R/L = 2\sqrt{3}. \tag{4.15}$$

This says that the two length scales R and L lock into a fixed ratio after a number of pairings. In the notation of (4.9) we would have $f = 2\sqrt{3}$.

Consider for $b = 2$ the equation, (4.8), for energy conservation during pairing

$$2\tilde{E}(\lambda_{n+1}) = \tilde{E}(\lambda_n) + (1/4\pi) \ln(L_{n+1}^2/L_n R_n). \tag{4.16}$$

For large n we can relate L_n to R_n and L_{n+1} to R_{n+1} by (4.15). Then, using (4.13), we see that $\tilde{E}(\lambda_n)$ converges to the fixed value $\tilde{E}^* = (1/8\pi) \ln(4/3) = 0.01145$. From equation (4.6) this corresponds to a value of $\lambda^* \simeq -0.945$, and to a universal, scaled vorticity profile P . The value of λ^* is close to -1 , the lower bound for λ , and the corresponding vorticity profile is very peaked. According to Lundgren & Pointin (1977), $\zeta(r)$ is then approximately $\zeta(0)/(1 + A(r/L)^2)^2$, where A is a scale factor. In the insert in figure 7 we have plotted contour lines of $1/(1 + r^2)^2$, roughly on the scale of the vortices in the simulation. Point plots like figures 4-5 and the data in table 1 show the vorticity distribution of a single finite area vortex to be a roughly circular cloud of points.

We do not want to claim very much for this theory. The general arguments still leave much to be explained and the one-dimensional model is not realistic. Furthermore, effects of fluctuations in Γ , L and R have not been taken into account. However, the idea that the vorticity distribution in a large turbulent structure is simply calculable from equilibrium statistical mechanics is important and is consistent with our numerical results. It suggests that all length scales based on a single structure do indeed lock into fixed ratios. The concept of an internal equilibrium of the shear layer also suggests novel theoretical approaches to the problem as discussed in §6.

5. Discussion

We are not aware of any experiments on a very long unsteady shear layer that are directly relevant to our numerical results. When we compare our simulation with mixing-layer experiments, a number of discrepancies are apparent. The intermittency factor on the midline of the simulation peaks at a value of about 0.65 as mentioned in §3 (*d*). This is much lower than experimental values for the mixing layer, where the intermittency factor on the axis is typically very close to unity. We attribute this mainly to effects of viscosity and vortex stretching in the mixing-layer experiments.

Our dimensionless values of peak velocity fluctuations are high compared to mixing-layer experiments. Furthermore, the transverse fluctuations are larger than the longitudinal fluctuations in our simulation. While this is also the case in the mixing layer at low Reynolds number (Browand & Weidman 1976), at high Reynolds number, which is the regime of our simulation, it is known that the reverse inequality holds (Wyganski & Fiedler 1970). The experiments, however, also tend to have velocity fluctuations in the spanwise or z direction of magnitude comparable to the y -velocity fluctuations, indicating a non-negligible degree of three-dimensionality in the flow. Thus, we do not really expect dimensionless ratios, calculated in our two-dimensional shear-layer simulation, to match high-Reynolds-number mixing-layer experiments. We recall that Ashurst (1977) had problems matching his two-dimensional mixing-layer simulation, which included viscous effects, to the low-Reynolds-number experimental results of Winant & Browand (1974).

Delcourt & Brown (1979) have recently produced a numerical simulation of the shear layer. They use 750 point vortices and an algorithm (the 'centre-to-centre method') that restricts the vortices to the sites of a grid at every time-step. Just as in the direct summation scheme the computation time scales as the square of the number of vortices. Their vorticity plots appear comparable to our figures 4–5, although we believe diffusive effects are larger in their simulation. They point out that using a simple Euler method time-stepping greatly enhances the effective viscosity for a cloud of like-signed vortices. Thus the earlier simulation by Ashurst (1977) could have had a much lower Reynolds number than intended. Already a second-order time-stepping method, and certainly the one used here in which the order was variable and typically equal to four, nearly eliminates this effect. Inspection of the pictures of Delcourt & Brown (1979) reveals some of the same scatter in the positions of the centres of the vortex blobs about the midline as we find. Ashurst's (1977) work displays virtually no scatter around the midline. Thus we tentatively suggest that this mechanism or mode becomes predominant as the Reynolds number increases. We intend to check this conjecture in the future.

We have run a number of internal consistency checks to demonstrate that our results reflect properties of two-dimensional turbulence and not numerical artifacts. To check the high fluctuation levels we have varied the wavenumber cut-off, described in §2, which effectively means altering the vorticity profile of the elementary vortices. This did not change the levels of fluctuation at all. We also took a vortex configuration from a 64×64 grid simulation and, in a purely static comparison, smoothed it onto a 32×32 grid and compared fluctuations. As one would expect, this operation did decrease the fluctuations but only by about 3%.

The peaked vorticity profiles observed in the simulation are qualitatively in accord

with the conditional sampling measurements of Browand & Weidman (1976). This is the only experiment, to our knowledge, in which a direct measurement of vorticity has been made. It is a low-Reynolds-number experiment, and it uses a conditional sampling technique that may have missed the qualitative feature of vortex scatter. The fragmented distribution of vorticity that we observe within the clusters in figures 4–7 for a single realization may well become a single-humped distribution in a conditionally sampled average. It would be interesting to see experimental technique refined to the point where vorticity contour plots, comparable to our figures 6 and 7, were readily produced.

Previous theoretical attempts at explaining the vortex dynamics of the shear layer become rather unconvincing in the light of our simulation. The model of Winant (see Winant & Browand 1974), which employs a juxtaposition of two exact solutions of a laminar shear layer due to Stuart (1967), is not dynamical since the resulting flow does not satisfy the equations of motion. Another shortcoming of this model, and related models based on the instability of a row of vortices (Saffman & Baker 1979), is the implication that the thickening proceeds in phase along the entire shear layer, i.e. is not statistical. The possibility of scatter about the midline is also not taken into account. The tearing mechanism of Moore & Saffman (1975), while plausible, apparently plays only a minor role. The vortices actually observed are not uniform but, as we have noted, very compact. Such blobs are more difficult to tear apart than the uniform vortices considered by Moore & Saffman (1975), and so this mechanism is suppressed. The most promising attempt at a simple theory is the one-dimensional vortex kinetics of Takaki & Kovaszny (1978). Their theory suffers from the same deficiency of ignoring the scatter as our one-dimensional shear-layer model in §4, but whereas we see a justification of simple scaling as an outstanding theoretical problem, Takaki & Kovaszny (1978) assume this scaling in solving their basic equation.

Apart from the numerical tests already mentioned, we have tried to assess to what degree a simulation, like the one at hand, can actually faithfully follow a flow that spans an ever widening range of scales. To address this question, the same configuration of vortices was run forward in time both on a 64×64 grid and on a 32×32 grid. The two simulations were run simultaneously and time-stepped together, and the spectrum of the difference of Fourier components of vorticity was monitored. Small scales are being treated very differently in these two simulations. The result is summarized in figure 17. For each wavenumber band $j < k < j + 1$, $j = 1, \dots, 17$, common to both grids, the histograms show the r.m.s. deviation of Fourier components of the two grid vorticities, i.e. a scale decomposed measure of the difference between the two simulations. The units on the ordinate are arbitrary but the same for all three histograms. The arrow above each histogram shows the location of the peak in the vorticity spectrum (3.10) of the 64×64 grid simulation. As the flow evolves this peak moves towards $k = 0$. Figure 17 demonstrates that the dominant wavenumber of vorticity apparently always manages to cascade back ahead of the receding front of the difference spectrum. Since even small relative shifts in the position of vortices from one simulation to the other, e.g. slight differences of phase in vortex merging events, will show up in the difference spectrum, it is understandable that the general height of this spectrum increases. Together with the result shown in figure 17 a favourable comparison of real space pictures produced from the two simulations seems to rule out the possibility, that errors on small scales are contaminating large

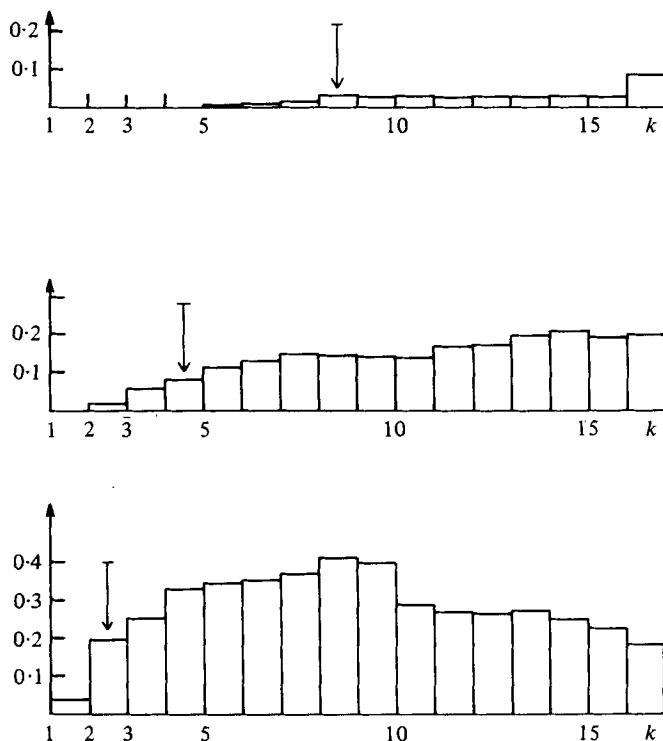


FIGURE 17. Growth of vorticity-difference spectrum for same vortex configuration time-stepped on two different grids. The arrows show the location of the peak in the vorticity spectrum, (3.10), or equivalently the dominant horizontal scale.

scale dynamics in any systematic way. This view is commonly held but rarely explicitly checked.

6. Summary and outlook

The plane shear layer is certainly the simplest of all free turbulent flows. Nevertheless, we believe it to be considerably more complicated than commonly held, even with the restriction to purely two-dimensional dynamics. We are convinced that large structures exist in the shear layer at some stage in its evolution, even when started from random initial conditions, but we can only speculate whether they persist indefinitely. When the large structures are present they introduce at least one new length scale, their size, which did not scale with the layer thickness during the course of our simulation. However, this violation of scaling did not show up when monitoring simple, low order velocity correlations functions. Thus, while the scaling predicted by self-preservation theory may be correct, the underlying dimensional arguments have become even harder to justify. The two-dimensional shear layer seems to thicken by a scattering of vortex structures about the midline and only partly by vortex amalgamation. The process of vortex disruption plays a very minor role if any. One might expect this picture to be explicable in terms of the governing conservation laws but so far such an explanation has escaped us. We do believe that the basic conserved

quantities are energy and L^2 (equation (2.1)), and that other inviscidly conserved quantities (like enstrophy) must adjust to these two.

The simple scaling of the shear layer is analogous to the large-scale similarity theory of Batchelor (1969) for the isotropic case, although this theory does not apply here due to the importance of L^2 . It is noteworthy that the dimensionless inverse cascade rate in this type of scaling, which in our case is r in equation (3.7), is apparently always a small number. This is possibly because an inviscid two-dimensional flow is severely constrained by many conservation laws, but the size of this parameter is not well understood. It is also not clear whether the existence of this small parameter can be used as a basis for theoretical calculation. It is important to note that the shear layer accomplishes an amazing reduction in the number of effective degrees of freedom as it evolves. Although we have not checked this in detail, we certainly expect that an array of point vortices, of the appropriate strengths, replacing the large vortex blobs would be capable of following the evolution of the shear layer to a high degree of approximation. We are presently considering algorithms that would take advantage of this feature, and thus would allow one to simulate an ever larger portion of an infinite shear layer using a fixed number of variables and equations of motion.

Although much remains unresolved from a fundamental point of view, the present paper has suggested a remarkably simple parametrization of the shear layer: The vortex blobs have a profile given by equilibrium statistical mechanics and their distribution about the midline can be taken as Gaussian. A result of this kind seems useful in applications.

We would like to thank J. L. Lumley for discussions and W. T. Ashurst for sending us a copy of his work (Ashurst 1977). The revised manuscript has profited from the comments and suggestions of G. L. Brown, F. K. Browand and N. J. Zabusky.

H. A. would like to thank the Cornell Graduate School for fellowship support.

This work was made possible by a direct grant of computing time by NCAR and was supported by NSF grant ATM-78-16411. NCAR is sponsored by the National Science Foundation.

Appendix. Derivation of equation (3.15)

From the definition of θ , equation (3.3),

$$\dot{\theta} = -2 \int dy \bar{u} \frac{\partial \bar{u}}{\partial t} / (\Delta U)^2. \tag{A 1}$$

Euler's equation for the x component of velocity,

$$\frac{\partial u}{\partial t} + u \frac{\partial u}{\partial x} + v \frac{\partial u}{\partial y} = -\frac{1}{\rho} \frac{\partial p}{\partial x}, \tag{A 2}$$

where ρ , p are density and pressure, gives

$$\frac{\partial \bar{u}}{\partial t} = -\frac{\partial}{\partial y} \overline{uv} \tag{A 3}$$

by statistical homogeneity in x and use of incompressibility. Substituting (A 3) into

(A 1), and integrating by parts, we get

$$\theta = \frac{2}{(\Delta U)^2} \left([\bar{u} \bar{v}] - \int dy \bar{v} \frac{\partial \bar{u}}{\partial y} \right) \quad (\text{A } 4)$$

But \bar{v} vanishes far below and far above the layer, and \bar{u} goes to a constant, so the integrated term vanishes. Furthermore, by homogeneity in x

$$\bar{\zeta} = -\frac{\partial \bar{u}}{\partial y}, \quad (\text{A } 5)$$

thus

$$\theta = 2 \int dy \bar{\zeta} \bar{v} / (\Delta U)^2, \quad (\text{A } 6)$$

which is (3.15).

REFERENCES

- ACTON, E. 1976 The modelling of large eddies in a two-dimensional shear layer. *J. Fluid Mech.* **76**, 561–592.
- ASHURST, W. T. 1979 Numerical simulation of turbulent mixing layers via vortex dynamics. In *Turbulent Shear Flows I* (ed. F. Durst, B. E. Launder, F. W. Schmidt & J. H. Whitelaw), pp. 402–413. Springer.
- BACHELOR, G. K. 1969 Computation of the energy spectrum in homogeneous two-dimensional turbulence. *Phys. Fluids*, Suppl. **12**, II 233–239.
- BATT, R. G. 1977 Turbulent mixing of passive and chemically reacting species in a low-speed shear layer. *J. Fluid Mech.* **82**, 53–95.
- BROWAND, F. K. & LATIGO, B. O. 1979 Growth of the two-dimensional mixing layer from a turbulent and nonturbulent boundary layer. *Phys. Fluids* **22**, 1011–1019.
- BROWAND, F. K. & TROUTT, T. R. 1980 A note on spanwise structure in the two-dimensional mixing layer. *J. Fluid Mech.* **97**, 771–781.
- BROWAND, F. K. & WEIDMAN, P. D. 1976 Large scales in the developing mixing layer. *J. Fluid Mech.* **76**, 127–145.
- BROWN, G. L. & ROSHKO, A. 1974 On density effects and large structure in turbulent mixing layers. *J. Fluid Mech.* **64**, 775–816.
- BUNEMAN, O. 1973 Subgrid resolution of flow and force fields. *J. Comp. Phys.* **11**, 250–268.
- CHANDRUSUDA, C., MEHTA, R. D., WEIR, A. D. & BRADSHAW, P. 1978 Effect of free-stream turbulence on large structure in turbulent mixing layers. *J. Fluid Mech.* **85**, 693–704.
- CHRISTIANSEN, J. P. 1973 Numerical simulation of hydrodynamics by the method of point vortices. *J. Comp. Phys.* **13**, 363–379.
- CHRISTIANSEN, J. P. & ZABUSKY, N. J. 1973 Instability, coalescence and fission of finite-area vortex structures. *J. Fluid Mech.* **61**, 219–243.
- DAMMS, S. M. & KÜCHEMANN, D. 1974 On a vortex-sheet model for the mixing between parallel streams. *Proc. Roy. Soc. A* **339**, 451–461.
- DEEM, G. S. & ZABUSKY, N. J. 1978 Vortex waves: Stationary ‘V states’, interactions, recurrence, and breaking. *Phys. Rev. Lett.* **40**, 859–862.
- DELCOURT, B. A. G. & BROWN, G. L. 1979 The evolution and emerging structure of a vortex sheet in an inviscid and viscous fluid modelled by a point vortex method. *2nd Symp. on Turbulent Shear Flows, Imperial College, London*, p. 14.35.
- DIMOTAKIS, P. E. & BROWN, G. L. 1976 The mixing layer at high Reynolds number: large-structure dynamics and entrainment. *J. Fluid Mech.* **78**, 535–560.
- FIEDLER, H. 1978 *Structure and Mechanisms of Turbulence*, I, II. Lecture Notes in Physics, volumes 75, 76. Springer.
- FRISCH, U., SULEM, P.-L. & NELKIN, M. 1978 A simple dynamical model of intermittent fully developed turbulence. *J. Fluid Mech.* **87**, 719–736.

- HOCKNEY, R. W., GOEL, S. P. & EASTWOOD, J. W. 1974 Quiet high-resolution computer models of a plasma. *J. Comp. Phys.* **14**, 148–158.
- KIDA, S. 1975 Statistics of the system of line vortices. *J. Phys. Soc. Japan.* **39**, 1395–1404.
- KOLMOGOROV, A. N. 1941 The local structure of turbulence in incompressible viscous fluid for very large Reynolds numbers. *C. R. Acad. Sci. U.S.S.R.* **30**, 301–305.
- KOLMOGOROV, A. N. 1962 A refinement of previous hypothesis concerning the local structure of turbulence in a viscous incompressible fluid at high Reynolds number. *J. Fluid Mech.* **13**, 82–85.
- KRAICHNAN, T.-H. 1967 Inertial ranges in two-dimensional turbulence. *Phys. Fluids* **10**, 1417–1423.
- LANDAU, L. D. & LIFSHITZ, E. M. 1969 *Statistical Physics*, section 75. Addison–Wesley.
- LEONARD, A. 1980 Vortex methods for flow simulation. *J. Comp. Phys.* (to appear).
- LUNDGREN, T. S. & POINTIN, Y. B. 1977 Statistical mechanics of two-dimensional vortices. *J. Stat. Phys.* **17**, 323–355.
- MICHALKE, A. 1964 Zur Instabilität und nichtlinearen Entwicklung einer gestörten Scherschicht. *Ing. Arch.* **33**, 264–276.
- MONIN, A. S. & YAGLOM, A. M. 1971 *Statistical Fluid Mechanics*, vol. 1 (ed. J. L. Lumley). Massachusetts Institute of Technology Press.
- MOORE, D. W. & SAFFMAN, P. G. 1975 The density of organized vortices in a turbulent mixing layer. *J. Fluid Mech.* **69**, 465–473.
- ONSAGER, L. 1949 Statistical Hydrodynamics. *Nuovo Cimento Suppl.* **6**, 279–287.
- ROSHKO, A. 1976 Structure of turbulent shear flows: A new look. *A.I.A.A. J.* **14**, 1349–1357.
- ROSSOW, V. J. 1977 Convective merging of vortex cores in lift-generated wakes. *J. Aircraft* **14**, 283–290.
- SAFFMAN, P. G. & BAKER, G. R. 1979 Vortex interactions. *Ann. Rev. Fluid Mech.* **11**, 95–122.
- SHAMPINE, L. F. & GORDON, M. K. 1975 *Computer Solution of Ordinary Differential Equations*. W. H. Freeman.
- STUART, J. T. 1967 On finite amplitude oscillations in laminar mixing layers. *J. Fluid Mech.* **29**, 417–440.
- TAKAKI, R. & KOVASZNY, L. S. G. 1978 Statistical theory of vortex merger in the two-dimensional mixing layer. *Phys. Fluids* **21**, 153–156.
- TENNEKES, H. & LUMLEY, J. L. 1972 *A First Course in Turbulence*. Massachusetts Institute of Technology Press.
- WINANT, C. D. & BROWAND, F. K. 1974 Vortex pairing: the mechanism of turbulent mixing-layer growth at moderate Reynolds number. *J. Fluid Mech.* **63**, 237–255.
- WYGNANSKI, I. & FIEDLER, H. E. 1970 The two-dimensional mixing region. *J. Fluid Mech.* **41**, 327–361.
- WYGNANSKI, I., OSTER, D., FIEDLER, H. & DZIOMBA, B. 1979 On the perseverance of a quasi-two-dimensional eddy-structure in a turbulent mixing layer. *J. Fluid Mech.* **93**, 325–335.
- ZABUSKY, N. J. 1977 Coherent structures in fluid dynamics. In *The Significance of Nonlinearity in the Natural Sciences*, pp. 145–205. Plenum Press.
- ZABUSKY, N. J., HUGHES, M. H. & ROBERTS, K. V. 1979 Contour dynamics for the Euler equations in two dimensions. *J. Comp. Phys.* **30**, 96–106.